UNIVERSIDADE FEDERAL DO RIO GRANDE DO SUL
FACULDADE DE AGRONOMIA
PROGRAMA DE PÓS-GRADUAÇÃO EM CIÊNCIA DO SOLO

O USO DO SENSORIAMENTO PRÓXIMO PARA ESTIMATIVA DE PROPRIEDADES DO SOLO DE IMPORTÂNCIA AGRÍCOLA E AMBIENTAL

JOÃO AUGUSTO COBLINSKI

(Tese de Doutorado)

UNIVERSIDADE FEDERAL DO RIO GRANDE DO SUL
FACULDADE DE AGRONOMIA
PROGRAMA DE PÓS-GRADUAÇÃO EM CIÊNCIA DO SOLO

O USO DO SENSORIAMENTO PRÓXIMO PARA ESTIMATIVA DE PROPRIEDADES DO SOLO DE IMPORTÂNCIA AGRÍCOLA E AMBIENTAL

JOÃO AUGUSTO COBLINSKI
Geógrafo (UNICENTRO)

Tese apresentada como um dos
requisitos à obtenção do Grau de
Doutor em Ciência do Solo

Porto Alegre (RS) Brasil
Março de 2021

CIP - Catalogação na Publicação

Coblinski, João Augusto
O USO DO SENSORIAMENTO PRÓXIMO PARA ESTIMATIVA DE PROPRIEDADES DO SOLO DE IMPORTÂNCIA AGRÍCOLA E AMBIENTAL / João Augusto Coblinski. -- 2021.
86 f.
Orientador: Élvio Giasson.

Tese (Doutorado) -- Universidade Federal do Rio Grande do Sul, Faculdade de Agronomia, Programa de Pós-Graduação em Ciência do Solo, Porto Alegre, BR-RS, 2021.

1. Espectroscopia de refletância. 2. Análise da textura do solo por espectroscopia de refletância. 3. Identificação da mineralogia do solo. 4. Quimiometria. 5. Machine-learning. I. Giasson, Élvio, orient. II. Título.

Elaborada pelo Sistema de Geração Automática de Ficha Catalográfica da UFRGS com os dados fornecidos pelo(a) autor(a).

JOÃO AUGUSTO COBLINSKI
Geógrafo – UNICENTRO
Mestre em Ciência do Solo – UFPR

TESE

Submetida como parte dos requisitos
para obtenção do Grau de

DOUTOR EM CIÊNCIA DO SOLO

Programa de Pós-Graduação em Ciência do Solo
Faculdade de Agronomia
Universidade Federal do Rio Grande do Sul
Porto Alegre (RS), Brasil

Aprovado em: 17/03/2021
Pela Banca Examinadora

Homologado em: 21/04/2021
Por

ELVIO GIASSON
Orientador-PPG Ciência do Solo

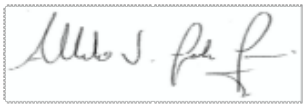

ALBERTO VASCONCELLOS INDA JUNIOR
Coordenador do
Programa de Pós-Graduação em
Ciência do Solo

TALES TIECHER
PPG Ciência do Solo - UFRGS
(MConf UFRGS)

FABRÍCIO DA SILVA TERRA
UFVJM
(MConf UFRGS)

GUSTAVO DE MATTOS VASQUES
EMBRAPA
(MConf UFRGS)

CARLOS ALBERTO BISSANI
Diretor da Faculdade
de Agronomia

Dedico a minha mãe, Marlene Cecato Coblinski (in memoriam).

AGRADECIMENTOS

Agradeço a minha família, especialmente minha nona Margarida Cecato, por seu apoio, amor e dedicação e aos meus tios, que incentivaram a estar aqui.

Ao professor Edivaldo L. Thomaz, meu orientador da graduação, onde me apresentou para a ciência do solo, e hoje estou terminando o doutorado nessa área devido a seu incentivo na base acadêmica. Agradeço também a professora Nerilde Favaretto, orientadora de mestrado, por todo seu apoio e ensinamentos. E agradeço também ao professor Élvio Giasson, que contribuiu muito para o meu crescimento profissional e o mais importante, crescimento pessoal. Ao professor Alberto V. Inda, pelos ensinamentos e grande apoio nos temas pesquisados. Ao professor José A. Demattê, pela oportunidade e grande contribuição nesse trabalho.

A todos os professores do PPGCS da UFRGS que se dedicam compartilhar seu conhecimento. A todos eu agradeço pelos ensinamentos e sem dúvida na ajuda de meu crescimento profissional.

Ao Programa de Pós-Graduação em Ciência do Solo/UFRGS, pela estrutura e recursos que possibilitaram o desenvolvimento deste trabalho e da realização do curso.

A CMPC Celulose Riograndense, por ter cedido a área de estudo e auxiliado dando suporte logístico e disponibilizando funcionários para auxiliar em coletas de amostras.

A todos os amigos que o doutorado me proporcionou e que levarei para toda a vida.

A Coordenação de Aperfeiçoamento de Pessoal de Nível Superior (CAPES), pela concessão da bolsa de estudos.

O USO DO SENSORIAMENTO PRÓXIMO PARA ESTIMATIVA DE PROPRIEDADES DO SOLO DE IMPORTÂNCIA AGRÍCOLA E AMBIENTAL[1]

Autor: João Augusto Coblinski
Orientador: Prof. Élvio Giasson

RESUMO

A necessidade por informações do solo de qualidade e com menor custo está crescendo e isso deve-se às demandas de planejamento do uso da terra e agricultura de precisão. Por causa disso, o sucesso das técnicas de sensoriamento próximo na estimativa das propriedades do solo está aumentando. As vantagens da análise de solos por espectroscopia de refletância incluem eficiência de tempo, conveniência econômica, aplicação não destrutiva e a redução do uso de agentes químicos envolvidos. Com isso, esta pesquisa propôs a aplicação do sensoriamento próximo, através da técnica de espectroscopia de refletância nas regiões VIS-NIR-SWIR e MIR (350-25000 nm), para avaliar a performance das diferentes regiões espectrais na quantificação das propriedades de solos. Dois estudos foram apresentados, sendo que o primeiro buscou avaliar diferentes regiões espectrais para a predição das frações granulométricas e o segundo teve como o objetivo identificar a composição mineralógica do solo e suas proporções nas regiões VIS-NIR-SWIR. Os estudos foram aplicados em solos do município de Pantano Grande, RS. Foram coletadas 197 amostras de solo. Os espectros do solo foram obtidos com FieldSpec Pro (VIS-NIR-SWIR) e por Alpha Sample Compartment RT (MIR) em laboratório. Nestes estudos, foi demonstrado que a técnica de espectroscopia de refletância é capaz de estimar as frações granulométricas do solo e complementar a análise padrão de textura do solo, principalmente quando um grande número de amostras de solo precisa ser tratado em um curto período de tempo. Permitindo também, avaliar a mineralogia do solo de forma rápida e com menor custo. As relações da mineralogia com a textura do solo permitem uma análise mais abrangente dos solos e uma rápida caracterização da área de estudo a fim de facilitar as tomadas de decisões que dê suporte na agricultura.

Palavras-chave: Espectroscopia de refletância, VIS-NIR, MIR, textura do solo, mineralogia do solo.

[1]Tese de Doutorado em Ciência do Solo. Programa de Pós-Graduação em Ciência do Solo, Faculdade de Agronomia, Universidade Federal do Rio Grande do Sul. Porto Alegre. (86p.) março de 2021.

THE USE OF PROXIMAL SENSING TO ESTIMATE SOIL PROPERTIES OF AGRICULTURAL AND ENVIRONMENTAL IMPORTANCE[2]

Author: João Augusto Coblinski
Adviser: Prof. Élvio Giasson

ABSTRACT

The necessity for quality and low-cost soil information is growing due to the demands of land use planning and precision agriculture. Because of this, the success of proximal sensing techniques in estimate soil properties is increasing. Advantages of soil spectroscopy include time efficiency, economic convenience, non-destructive application and reducing the use of chemical agents involved. With this, this research proposes the application of proximal sensing, through the technique of reflectance spectroscopy in the VIS-NIR-SWIR and MIR (350-25000 nm) regions, to evaluate the performance of the different spectral regions in the quantification and semi-quantification of soil properties. Two studies were presented, the first of which sought to evaluate different spectral regions for the prediction of soil texture and the second, aimed to identify the mineralogical composition of the soil and its proportions through VIS-NIR-SWIR regions. The studies were conducted in Pantano Grande, RS, Brazil. 197 soil samples were collected. The soil spectra were obtained with FieldSpec Pro (VIS-NIR-SWIR) and by Alpha Sample Compartment RT (MIR) in the laboratory. In these studies, it was demonstrated that the reflectance spectroscopy technique is able to predict the soil texture contents and complement the standard soil particle size analysis, especially when a large number of soil samples need to be treated in a short period of time. It also allows to assess the soil mineralogy quickly and at a lower cost. The relationship between mineralogy and soil texture allows for a more comprehensive analysis of soils and a quick characterization of the study area in order to facilitate decision-making that supports agriculture.

Keywords: Reflectance spectroscopy, VIS-NIR, MIR, soil texture, soil mineralogy.

[2]Doctoral thesis in Soil Science. Graduate Program in Soil Science, Faculty of Agronomy, Universidade Federal do Rio Grande do Sul. Porto Alegre. (86p.) March 2021.

SUMÁRIO

RELAÇÃO DE TABELAS

RELAÇÃO DE FIGURAS

1. Introdução Geral

A demanda por informações detalhadas sobre o solo para auxiliar na tomada de decisão agrícola, servindo de apoio para uma produção sustentável, está aumentando (SIQUEIRA et al., 2015). Para melhor conhecer o solo, suas propriedades e seus processos, os quais variam espacialmente e temporalmente, há a necessidade de métodos eficazes para sua mensuração e seu monitoramento. Os métodos convencionais são caros e muitas vezes impraticáveis, pela demora que pode ocorrer dependendo da quantidade de amostras requeridas, além de necessitarem de preparação de amostras com agentes nocivos (VISCARRA ROSSEL et al., 2016).

Assim, tem-se necessidade de técnicas e procedimentos analíticos simples e rápidos que possam substituir os métodos convencionais dispendiosos e demorados (RAMAROSON et al., 2017). Nas últimas décadas, tecnologias vêm sendo incorporadas por cientistas do solo com enfoque na agricultura de precisão e na pedologia, a fim de melhorar a compreensão da distribuição dos solos e suas propriedades na paisagem (DEMATTÊ E SILVA TERRA, 2014), assim como pensar em métodos para aliar o aumento da produtividade do solo e a diminuição da degradação ambiental (MA et al., 2019). Essas tecnologias visam, também, à complementação ou à substituição dos métodos convencionais, buscando manter a integridade da amostra de solo, melhorar a rapidez e a sensibilidade da análise e diminuir o custo (JANIK; SKJEMSTAD; MERRY, 1998) e o uso de extratores químicos para a preparação das amostras (VISCARRA ROSSEL et al., 2006).

Com isso, deu-se enfoque a estudos e à inclusão do sensoriamento remoto e próximo na ciência do solo, que se baseiam na aquisição de informações de um objeto sem ter contato direto, por meio de sensores de laboratório, campo ou órbita. Um exemplo disso é a espectroscopia de refletância (ER), uma técnica em que a energia eletromagnética funciona como um agente que se inter-relaciona com os componentes do solo. Essa relação trata-se de um processo físico no qual, basicamente, o solo pode absorver energia e refletir parte dessa energia total incidente. A absorção da energia pelo solo é dada em função dos materiais que o compõem, os quais absorvem energia de forma distinta e em diferentes comprimentos de onda. As frequências das vibrações moleculares dos componentes do solo ocorrem na faixa do visível (VIS), de 350-700 nm, no infravermelho próximo e de ondas curtas (NIR-SWIR), de 700-2500 nm, e infravermelho médio (MIR), no comprimento de onda de 2500 a 25000 nm (4000-400 cm^{-1}) (VISCARRA ROSSEL et al., 2006).

Estudos que utilizam a espectroscopia de refletância como técnica para predição das propriedades do solo vêm crescendo muito na última década. Porém, esta pesquisa buscou completar lacunas de trabalhos anteriores, com o objetivo de entender qual região espectral é melhor para estimativa das propriedades do solo em regiões tropicais e subtropicais e o que configura tal região como a mais adequada, analisando o que influenciou nos modelos de predição. Outro objetivo de estudo de suma importância em solos dos trópicos é caracterizar a composição mineralógica do solo de forma eficiente e rápida, por meio das assinaturas espectrais dos minerais, já que a mineralogia tem grande influência nas propriedades físicas e químicas do solo.

Com isso, esta pesquisa propõe a aplicação do sensoriamento próximo, através da técnica de espectroscopia de refletância nas regiões VIS-NIR-SWIR e MIR (350-25000 nm), para avaliar a performance das diferentes regiões espectrais na quantificação e na semiquantificação das propriedades de solos.

Os objetivos específicos são: i) explorar as possibilidades de quantificação do conteúdo das frações granulométricas (argila, areia e silte) em diferentes regiões espectrais, ii) comparar o desempenho de diferentes abordagens do conjunto de amostras e iii) identificar as principais composições mineralógicas de solos tropicais e subtropicais do Sul do Brasil, através da

espectroscopia de refletância, agrupando as amostras por classes texturais do solo.

No primeiro capítulo, é apresentada uma revisão bibliográfica sobre a espectroscopia de refletância, seu princípio e os principais estudos na ciência do solo. Além disso, faz-se um panorama sobre as duas propriedades do solo abordadas na tese, isto é, a textura e a mineralogia do solo, apresentando os conceitos, a importância e a influência no sistema solo, assim como a influência nas curvas espectrais.

No segundo capítulo, é apresentado um estudo que buscou avaliar a performance de diferentes regiões espectrais (VIS-NIR-SWIR e MIR – 350 nm a 25000 nm) para a predição de frações granulométricas do solo. Os conteúdos de argila, silte e areia foram estimados através de duas distintas regiões espectrais (VIS-NIR e MIR) e da fusão destas. Os modelos de predição foram testados de duas maneiras: com o conjunto de amostras em sua totalidade e com as amostras separadas por profundidade do solo, utilizando o algoritmo *cubist* para treinar e validar os modelos.

No terceiro capítulo, a espectroscopia de refletância nas regiões VIS-NIR-SWIR (350-2500 nm) foi utilizada para a identificação da composição mineralógica do solo e da abundância relativa dos minerais. A espectroscopia pode ser uma alternativa acessível para suprir a demanda por uma análise mineralógica mais rápida a custo menor, ao ser comparada à técnica padrão. O conjunto de amostras foi separado em função das classes texturais para facilitar a identificação das assinaturas espectrais dos minerais. Para essa identificação, foram realizados dois tipos de pré-processamentos na curva espectral, bem como curvas espectrais de minerais puros retirados da biblioteca espectral da United States Geological Survey (USGS).

2. CAPÍTULO I – Revisão Bibliográfica

2.1. Espectroscopia de refletância

O sensoriamento próximo baseia-se na aquisição de informações de um objeto sem contato direto, por meio de sensores instalados em laboratório ou em campo. Esses sensores podem realizar uma diversidade de análises do solo, como, por exemplo, condutividade elétrica do solo, umidade, resistência mecânica do solo, além de, através da capacidade de absorver e refletir energia eletromagnética, análise de inúmeros atributos do solo, como textura do solo, mineralogia, nutrientes, elementos tóxicos, etc (VISCARRA ROSSEL et al., 2011).

Dentre esses sensores proximais, encontra-se a técnica da espectroscopia de refletância (ER), a qual se utiliza do espectro eletromagnético para analisar o comportamento de um objeto. Na ER, a energia incidente de uma fonte interagirá com a superfície de um objeto, sendo que parte dessa energia pode ser absorvida pela amostra, e a outra parte, refletida. A quantidade de energia que será refletida ou absorvida pelo solo é dada em função dos materiais que o compõem, tendo diferentes interações, dependendo de suas propriedades físicas, químicas e mineralógicas (BOWERS; HANKS, 1965). A absorção da energia pelo objeto pode ocorrer de duas formas: pelo processo de transição eletrônica e pelo processo vibracional. A transição eletrônica dá-se quando a energia incide sobre um átomo, de modo a excitar seus elétrons, que se transacionam para um nível orbital menor, emitindo um fóton. Quando um átomo absorve um fóton de um dado comprimento de onda, seus elétrons movem-se de um nível orbital menor para um maior

Já o processo vibracional se deve às vibrações das ligações moleculares, ou seja, quando a energia incide sobre uma molécula, ela excita as ligações que as vibram e absorvem a energia. A massa da molécula e a força de cada ligação molecular determinarão sua frequência de vibração no espectro eletromagnético (FANG et al., 2018; HUNT; SALISBURY, 1970).

O espectro eletromagnético é o conjunto de todas as frequências eletromagnéticas que existem, como ondas de rádio, micro-ondas, infravermelho, luz visível e ultravioleta, raios x e raios gama. Porém, a ER opera apenas na frequência do infravermelho e da luz visível, sendo dividida nas regiões do visível – VIS (350- 700 nm), infravermelho próximo – NIR (700-1100 nm), infravermelho de ondas curtas – SWIR (1100-2500 nm) e infravermelho médio – MIR (2500 – 25000 nm/4000-400 cm^{-1}) (VISCARRA ROSSEL et al., 2011).

Na região do visível (VIS), ocorrem as transições eletrônicas, pois as absorções dessa radiação ocorrem sob altas energias. Já na região do infravermelho próximo e de ondas curtas (NIR-SWIR), não se tem energia suficiente para induzir transições eletrônicas. Devido a isso, as absorções dessas regiões são restritas a compostos com menores diferenças de energia nos estados vibracionais. Contudo, é na região do infravermelho médio (MIR) que as transições vibracionais atuam, tendo muitas características de absorção. Já na região NIR-SWIR, são detectados apenas os sobretons e as combinações dessas vibrações, caracterizados por modos vibracionais amplos, fracos e muitas vezes sobrepostos, levando essa região a ter poucas características de absorção (STENBERG et al., 2010; VISCARRA ROSSEL et al., 2011).

A ER em nível de laboratório começou a ser utilizada em estudos da ciência do solo nos anos de 1950, por Brooks (1952), quando estudaram a radiação atmosférica e seu reflexo no solo, e, mais tarde, nos anos de 1960, por Bowers e Hanks (1965), que avaliaram e determinaram os fatores que influenciavam a refletância da energia eletromagnética dos solos. Posteriormente, nos anos 1970, Hunt e Salisbury (1970) determinaram os espectros na faixa do visível (VIS) e do infravermelho próximo (NIR) de minerais silicatados. Porém, foi somente nas últimas três décadas que a espectroscopia de refletância despertou interesse pela sua utilidade e importância na ciência do

solo, fato que se deve ao avanço de técnicas estatísticas multivariadas e softwares de programação, como o R e Python (VISCARRA ROSSEL et al., 2006, 2011).

As regiões da espectroscopia de refletância são sensíveis nas fases orgânicas e inorgânicas do solo, tornando-se muito úteis para identificação e estimativa dessas propriedades e avaliação das variações espaciais e em profundidade do solo (DEMATTÊ et al., 2014; VISCARRA ROSSEL et al., 2006). Diferentes estudos, voltados à ciência do solo utilizando a técnica de ER, estão sendo realizados, como, por exemplo: estimativa do conteúdo das frações granulométricas do solo, em que Tümsavaş et al. (2018) tiveram como objetivo a predição das frações argila e areia nas regiões VIS-NIR-SWIR em campo irrigado, na Turquia, alcançando um valor médio de validação de R^2 para argila de 0,86, enquanto, para areia, R^2 de 0,83. Jiang et al. (2017) realizaram a estimativa do nitrogênio do solo em regiões montanhosas, na China, através das regiões VIS-NIR-SWIR, e alcançaram R^2 de 0,88 para validação do modelo.

Knox et al. (2015) tiveram como objetivo a predição das frações do carbono do solo com a espectroscopia de refletância nas regiões VIS-NIR-SWIR e MIR, em solos dos Estados Unidos, alcançando resultados significativos para todas as frações, como carbono total, carbono orgânico do solo, carbono recalcitrante e carbono hidrolisável. Munawar et al. (2020) utilizaram a região NIR-SWIR para estimar as propriedades que indicam a fertilidade do solo, tais quais: nitrogênio, fósforo, cálcio, potássio, magnésio e o pH do solo em campos de arroz, na Indonésia. Eles encontraram resultados significativos para validação dos modelos, indicando que a técnica pode ser usada para determinar os parâmetros de fertilidade do solo.

Morellos et al. (2016) alcançaram bons resultados (R^2>0,7) para a predição do conteúdo de água com espectroscopia na região VIS-NIR, analisando diretamente a campo na Alemanha. Ramaroson et al. (2017) aplicaram a espectroscopia de refletância para estimar a mineralogia do solo em Madagascar, concluindo que essa técnica pode ser usada para uma análise rápida com uma acurácia aceitável. Zhao et al. (2017) aplicaram a técnica para analisar o intemperismo do solo, buscando correlações entre bandas relacionadas aos minerais do solo com diferentes índices de intemperismo na

China. Terra et al. (2018) utilizaram a espectroscopia de reflectância para realizar avaliações pedológicas no solo, como levantamento e classificação do solo e determinação de níveis de intemperismo em solos nos estados de São Paulo, Minas Gerais, Mato Grosso do Sul e Goiás. Gholizadeh et al. (2020) avaliaram elementos potencialmente tóxicos para o solo, como cromo, cobre, alumínio, chumbo e zinco, através da espectroscopia de refletância em mais de 2000 amostras de solo de solos florestais distribuídos em toda a República Tcheca.

Essas estimativas são possíveis porque, através da espectroscopia de refletância, é possível identificar assinaturas espectrais específicas de alguns atributos do solo, como óxidos de ferro (hematita e goetita) (FANG et al., 2018; SCHEINOST et al., 1998; SELLITTO et al., 2009; TORRENT; BARRÓN, 2002), argilominerais (CLARK et al., 1990; MADEIRA et al., 1995; MELO; WYPYCH, 2009; STENBERG et al., 2010), quartzo (CALDERÓN; MIKHA; VIGIL, 2011; LANDRÉ et al., 2018), carbono orgânico do solo (CAMBOU et al., 2016; VAŠÁT et al., 2017a), água higroscópica (WIGHT; ASHWORTH; ALLEN, 2016), entre outras.

2.2. Análise de textura do solo por espectroscopia de refletância

A textura do solo é a classificação de solos baseada na proporção relativa das partículas minerais de um solo que constituem a fração terra fina (< 2 mm). Os tamanhos dessas partículas variam desde aquelas vistas a olho nu até aquelas abaixo do alcance de um microscópio de alta potência (BROWN, 2011). As categorias de tamanho mais comumente utilizadas são: argila (< 0,002 mm), silte (0,002 -0,05 mm) e areia (0,05 – 2 mm) (FAO, 2015).

O tamanho da partícula irá definir a proporção entre microporos e macroporos, determinando, assim, a área de contato entre as partículas sólidas e a água (KLEIN et al., 2010). Embora um solo de textura argilosa tenha maior estabilidade de agregados comparado a solos arenosos, uma vez destacadas, as partículas de argila são mais facilmente carreadas pelo escoamento superficial devido ao seu tamanho; porém, são as partículas de areia que são

mais facilmente destacadas por serem menos coesas (BLANCO-CANQUI; LAL, 2010).

A argila é a fração mais fina do solo, é a fração coloidal; com isso, ela é altamente reativa, tem grande área superficial específica e alta densidade de cargas. Essa fração pertence ao grupo de minerais conhecidos como alumino-silicatos (minerais secundários), que são formados através do intemperismo dos minerais primários contidos na rocha. Por sua vez, também contém partículas finas de óxido de ferro (Fe_2O_3), óxido de alumínio (Al_2O_3) e carbonato de cálcio ($CaCO_3$) (HILLEL, 1998; LAL, 2004). A fração de areia é dividida em areia grossa, média e fina. Os grãos de areia geralmente consistem em quartzo (SiO_2), mas também podem ser fragmentos de feldspato e mica. Essa fração tem baixa área superficial específica, tendo, como consequência, baixa capacidade de retenção de água e nutrientes. O silte consiste em partículas de tamanho intermediário entre areia e argila. A composição mineralógica do silte é semelhante à da areia, mas o silte tem área de superfície maior, e suas partículas, muitas vezes, são revestidas com argila fortemente aderente, podendo exibir, em um grau limitado, alguns dos atributos físico-químicos da argila (HILLEL, 1998; LAL, 2004).

A textura do solo é de suma importância e influencia em tomadas de decisão agrícola. Conjuntamente com outras características do solo, pode definir práticas agrícolas que condizem com a condição específica do solo analisado. Para realizar a classificação da textura do solo, estipulada com base no triângulo textural, devem ser quantificados os tamanhos de partículas através da análise da granulometria do solo, para a qual existem duas metodologias-padrão que são utilizadas até hoje: o método da pipeta e o método do densímetro. O método da pipeta fundamenta-se na velocidade de deslocamento vertical das partículas do solo. Já o método do densímetro consiste na sedimentação das partículas, sendo que a densidade da concentração total de argila é determinada após a adição de um dispersante químico. Nos dois métodos, a fração silte é determinada por diferença (TEIXEIRA et al., 2017).

Apesar dessas metodologias serem bem aceitas, precisas e utilizadas há décadas, podem ser demoradas em suas análises, tornando-se dispendiosas quando se tem a necessidade de análise de um grande conjunto de amostras.

Esses são os motivos pelos quais a técnica de espectroscopia de refletância nas regiões do VIS-NIR-SWIR e MIR é vista como uma alternativa devido às suas vantagens, que incluem rapidez, menor custo, análise não invasiva e uso reduzido de agentes químicos (VISCARRA ROSSEL et al., 2016).

Muitos estudos de quantificação da granulometria do solo por espectroscopia de refletância foram e vêm sendo desenvolvidos nos últimos anos, trazendo bons resultados, devido à grande influência que as partículas do solo têm sobre as ondas eletromagnéticas nas regiões VIS-NIR-SWIR e MIR. Essa influência deve-se principalmente aos argilominerais e óxidos que compõem essas partículas, com características de absorção específicas na curva espectral (RAMAROSON et al., 2017; SORIANO-DISLA et al., 2014).

A fração argila, como já citado, é composta de minerais secundários, incluindo argilominerais, óxidos de ferro e de alumínio (LAL, 2004), componentes que têm grande resposta na espectroscopia de refletância, mostrando assinaturas espectrais nas regiões VIS-NIR-SWIR e MIR. Os óxidos de ferro têm assinaturas espectrais na região do visível (VIS), como a goetita (Gt) em 420 e 480 nm e a hematita (Hm) em aproximadamente 520 e 650 nm, e na região NIR, sendo em ~920 nm para Gt (DEMATTÊ et al., 2014; SCHEINOST et al., 1998; VISCARRA ROSSEL; BEHRENS, 2010). O óxido de alumínio gibsita (Gb) tem suas assinaturas espectrais tanto na região SWIR (2265 nm) quanto na região MIR em aproximadamente 3500 cm^{-1} (DEMATTÊ et al., 2014; NGUYEN; JANIK; RAUPACH, 1991; TINTI et al., 2015). Já os argilominerais podem ser identificados por suas assinaturas espectrais na região NIR-SWIR, entre 2200 e 2500 nm (XU et al., 2017; YU; HUNT, 2018), referindo-se à caulinita (Kt) ou à esmectita (Sm). Na região MIR, a Kt apresenta assinaturas espectrais entre 3600 e 3700 cm^{-1} (DJOMGOUE; NJOPWOUO, 2013). A areia, composta principalmente de quartzo (SiO_2), não tem assinaturas espectrais nas regiões VIS-NIR-SWIR, porém influencia na curva espectral como um todo, aumentando a intensidade de refletância (DEMATTÊ, 2002; DEMATTÊ et al., 2014). No entanto, na região MIR, o quartzo apresenta características específicas em ao menos três bandas, sendo em aproximadamente 1100 cm^{-1}, 1180 cm^{-1} e 2000 cm^{-1}, causando também aumento na intensidade de refletância se em grande

quantidade no solo (JANIK; FORRESTER; RAWSON, 2009; MA et al., 2019; SALISBURY; D'ARIA, 1992).

Já a fração silte, como constatado em estudos anteriores, não apresenta características específicas em espectros de solos. Em trabalho que teve como objetivo estimar vários atributos físicos e químicos do solo, Zhang et al. (2017) encontraram também baixa acurácia para predição de silte, com fraca correlação com outras propriedades do solo. Segundo esses autores, o motivo desse resultado é que o silte não possui características espectrais reconhecíveis na região VIS-NIR-SWIR. Utilizando a mesma região espectral, Curcio et al. (2013) realizaram a predição da textura do solo com bandas específicas relacionadas a argilominerais e ao quartzo, para argila e areia, porém não encontraram característica relacionada à fração silte e realizaram a quantificação desta por diferença entre argila e silte. Já para outros autores, os resultados não significativos do silte se devem a outro fator. Pinheiro et al. (2017), trabalhando com predição de atributos físicos e químicos, inclusive a textura do solo, em que utilizaram o método da pipeta como método padrão, também encontraram baixa acurácia para o silte. O mesmo resultado insatisfatório pode ser encontrado por Madari et al. (2006), que determinaram a textura por densímetro. Segundo esses autores, os resultados pobres encontrados para a predição de silte se devem à metodologia padrão empregada. Tanto o método da pipeta quanto o do densímetro determinam a fração silte do solo pela diferença do valor de argila e areia, o que significa que os erros analíticos das medições de argila a areia são propagados para a fração do silte.

Com o avanço da técnica da espectroscopia de refletância, muito interesse vem sendo despertado para análise dos atributos do solo, inclusive a textura. Estudos sobre a textura já foram realizados em todas as regiões espectrais, por meio de comparações entre elas, fusão das regiões ou apenas predição do conteúdo da textura do solo com uma região espectral. O primeiro estudo relacionado à predição do conteúdo das partículas do solo ocorreu em 1995, com a predição da fração argila através da região espectral MIR (JANIK; SKJEMSTAD, 1995) em amostras de diferentes localidades. Os autores realizaram a predição e encontraram valores de validação de $R^2 = 0,87$. Desde então, os estudos continuaram sendo realizados em diferentes regiões

espectrais. Vendrame et al. (2012) analisaram um conjunto de 148 amostras de diferentes profundidades através da espectroscopia na região NIR (1100 – 2500 nm), alcançando um R^2 de validação de 0,74, 0,46 e 0,72 para argila, silte e areia respectivamente. Curcio et al. (2013) construíram um modelo de predição de textura do solo com 100 amostras através das regiões VIS-NIR-SWIR. Eles encontraram resultados de R^2 de 0,87 para argila, 0,80 para areia e 0,6 para silte.

Além de diferentes regiões espectrais, autores testam diferentes tipos de algoritmos para realizar a predição de textura do solo, como Partial Least Squares Regression (PLSR). Wang et al. (2014) estimaram os teores da textura do solo através das regiões VIS-NIR-SWIR, na China, utilizando o PLSR, chegando a alcançar acurácia de validação de R^2 = 0,72, 0,58 e 0,79 para argila, silte e areia, respectivamente. Pinheiro et al. (2017), com a mesma região espectral do estudo anterior, estimaram a predição da textura do solo utilizando o algoritmo PLSR no norte do Brasil, onde alcançaram R^2 = 0,78, 0,36 e 0,62 para argila, silte e areia, respectivamente. Vasava et al. (2019) realizaram a predição da textura do solo em diferentes localidades na Índia através da espectroscopia na região VIS-NIR-SWIR, com o PLSR, tendo alcançado acurácia de R^2 = 0,77 e 0,80 para argila e areia respectivamente. Outro algoritmo utilizado é o Support Vector Machine (SVM). Silva et al. (2019), com um grande conjunto de dados do sul do Brasil, estimaram as frações argila e areia na região VIS-NIR-SWIR com diferentes algoritmos, dentre os quais o SVM, tendo encontrado R^2 = 0,77 para argila e 0,67 para areia, sendo o algoritmo menos acurado dentre 5 utilizados. Outro algoritmo também utilizado é o Artificial Neural Network (ANN). Wijewardane et al. (2018) estimaram diversos atributos do solo, dentre os quais a textura através da espectroscopia na região MIR e com a utilização de ANN. Eles usaram uma biblioteca da região espectral MIR com mais de 20.000 amostras, alcançando acurácia de R^2 = 0,77, 0,73 e 0,75 para argila, silte e areia, respectivamente. Com o algoritmo Cubist, Zhang et al. (2017) estimaram a textura do solo em uma área agrícola no Canadá, através da espectroscopia na região VIS-NIR-SWIR, alcançando acurácia de R^2 = 0,70, 0,00 e 0,50 para argila, silte e areia, respectivamente. Outro algoritmo utilizado é o Random Forest (RF). Benedet et al. (2020) estimaram a textura do solo com a região VIS-NIR-SWIR em território brasileiro, em três estados, por meio do RF, alcançando R^2 entre 0,7 e 0,8 para areia e argila, respectivamente.

Também são utilizados diferentes tipos de pré-processamentos da curva espectral, como, por exemplo, continuum removal, por meio do qual Curcio et al. (2013) estimaram a textura do solo através da região VIS-NIR-SWIR, em solos agrícolas e florestais na Itália, realizando o pré-processamento do continuum removal na curva espectral para correlacionar as características de absorção com as frações da textura. Com isso, alcançaram valores de acurácia não satisfatórios, sendo R^2 = 0,68, 0,12 e 0,17 para argila, silte e areia respectivamente. Pré-processamentos com a primeira e a segunda derivadas também são muito utilizados, como no estudo de Vendrame et al. (2012), que realizam a estimativa da textura com os espectros pré-processados na primeira e segunda derivada, alcançando resultados acurados apenas para argila (R = 0,74). Viscarra Rossel et al. (2009) avaliaram diferentes pré-processamentos para a calibração do modelo, sendo que o melhor encontrado foi a primeira derivada, usada para processar as curvas e realizar a predição do conteúdo de argila no solo, alcançando R^2 de 0,78. Também existem outros processamentos utilizados, tais como: absorbância, suavização, SNV (Standard Normal Variate), MSC (Multiplicative Scatter Correction), normalização, entre outros.

Todas essas técnicas de processamentos e algoritmos são testadas para buscar uma melhor performance de dados espectrais na modelagem da estimativa das frações granulométricas do solo. O pré-processamento da curva espectral é realizado para melhorar os resultados de calibração e validação do modelo para predição. Entretanto, como na imensa maioria dos trabalhos se usam os pré-processamentos, não sabemos se realmente trouxeram melhores resultados do que modelos realizados através de espectros brutos.

2.3. Análise da mineralogia do solo por espectroscopia de refletância

A composição mineralógica em solos tropicais e subtropicais, independentemente do material de origem, dá-se principalmente pela presença de óxidos de ferro e argilominerais 1:1 (OLIVEIRA et al., 2020). Os óxidos, hidróxidos e oxihidróxidos de ferro, mais conhecidos apenas como óxidos de Fe, são considerados os mais abundantes óxidos metálicos nos solos. Esses minerais têm grande poder pigmentante no solo, influenciando diretamente na sua cor, como vermelho, amarelo, laranja ou marrom. Os óxidos de ferro são

considerados o segundo grupo mais importante de minerais da fração argila em solos tropicais e subtropicais, ficando atrás apenas dos argilominerais 1:1, como a caulinita (BIGHAM; FITZPATRICK; SCHULZE, 2002; COSTA; BIGHAM, 2009).

A concentração de óxidos de ferro no solo depende do seu teor no material de origem e do grau de intemperismo do solo, sendo que suas proporções variam com a temperatura e a umidade, e seus níveis em solos subtropicais brasileiros variam tipicamente de poucas gramas a 100 $g.kg^{-1}$ (BIGHAM; FITZPATRICK; SCHULZE, 2002; OLIVEIRA et al., 2020). Os óxidos ocorrem em partículas muito pequenas e têm alta área superficial específica. Devido a isso, atuam com eficiência na adsorção de ânions, cátions e influenciam também no aumento da microporosidade e na cimentação de outros componentes do solo (COSTA; BIGHAM, 2009; GHIDIN et al., 2006).

Os óxidos de Fe nos solos são minerais primários, como a magnetita e a ilmenita, encontrados frequentemente nas frações silte e areia, ou minerais secundários resultantes do processo de intemperismo químico, encontrados na fração argila (COSTA; BIGHAM, 2009). Os óxidos de ferro que mais ocorrem nas regiões subtropicais são a hematita e a goetita, cuja ocorrência normalmente é associada. A hematita ocorre em ambientes de altas temperaturas, em solos de drenagem livre, com baixa concentração de matéria orgânica, e concede cores avermelhadas ao solo. Quanto à goetita, sua formação é favorecida em ambientes frios e úmidos ou em ambientes que facilitam o acúmulo de água (COSTA; BIGHAM, 2009; VENDRAME et al., 2011), concedendo cores mais amareladas ao solo.

Outro principal grupo de minerais em solos tropicais e subtropicais é o grupo dos argilominerais 1:1, sendo a caulinita o mais importante mineral desse grupo em solos brasileiros. Apesar da baixa CTC e da área superficial específica, altos teores de caulinita são encontrados na fração argila, tornando-a o mineral de maior importância no comportamento químico dos solos tropicais (KÄMPF; CURI; MARQUES, 2009). A caulinita é formada principalmente em ambientes de intenso intemperismo químico e lixiviação de cátions básicos, como, Ca^{2+}, Mg^{2+}, K^{+}, Na^{+} e também SiO_2. O seu processo de formação é principalmente por dissolução de minerais primários e reprecipitação do Si e do Al pela solução do

solo, predominante nas regiões de clima quente e úmido (MELO; WYPYCH, 2009).

A análise da mineralogia do solo é usualmente realizada pela difratometria de raios x, que é considerada a principal técnica para a identificação de minerais, sendo a técnica padrão. É essencial para a caracterização mineralógica dos argilominerais. Porém, meios alternativos estão sendo estudados para a análise mineralógica, e um desses meios é a espectroscopia de refletância. Isso porque a análise por DRX tem alto custo e requer muito tempo de processamento das amostras.

Os minerais mais estudados através da espectroscopia de refletância são os óxidos de ferro. Eles apresentam assinaturas espectrais distintas na região do visível (350-700 nm) e características são observadas também no infravermelho próximo (700-1100 nmm). A goetita tem suas características de absorção na região do visível nas bandas de 420 e 480 nm; já na região NIR, é identificada na banda de 920 nm e com uma fraca absorção a 1700 nm, que se refere aos grupos OH da estrutura cristalina da goetita. Para a hematita, suas características de absorção na região VIS ocorrem por volta de 520 e 650 nm e, na região NIR, ocorre em 880 nm (FANG et al., 2018; STENBERG et al., 2010).

Os argilominerais 1:1 também têm suas características de absorção espalhadas na região VIS-NIR-SWIR. A caulinita, principal argilomineral 1:1 em solos tropicais e subtropicais, é caracterizada com absorções nas bandas de 1400, 2200 e 2165 nm, porém, a banda específica que identifica esse mineral é por volta de 2200 nm, com um pico intenso de absorção. Nessa mesma região, podem ser identificados outros argilominerais, mas, para diferenciá-los da caulinita, pode ser observado um característico ombro que se forma na banda de 2165 nm (CLARK et al., 1990; VISCARRA ROSSEL et al., 2010). Os argilominerais 2:1 apresentam características acima de 2300 nm. Em solos subtropicais, principalmente na região sul do Brasil, esses minerais são apenas remanescentes do intemperismo. Assim, eles estarão em pequenas quantidades nesses solos e não apresentarão uma grande influência na curva espectral, tendo fracas características de absorção, embora ainda notáveis (CLARK et al., 1990; JACKSON; SHERMAN, 1953; XU et al., 2017; ZHAO et al., 2017).

Bahia et al. (2015) realizaram estudo para estimar os teores de hematita e goetita de solos da camada superficial, em áreas de cana-de-açúcar, no estado de São Paulo, comparando os métodos de Difratometria de Raios X (DRX) e Espectroscopia de Refletância (ER). Eles identificaram que a análise dessas frações da mineralogia por DRX realmente tem maior gasto em tempo, reagentes e, consequentemente, dinheiro. Para a análise de DRX, o tempo gasto para realizar uma amostra de Hm e Gt foi de 55 horas e 30 minutos. Isso envolve: separação da argila (~24 horas), concentração de óxidos com NaOH (~24 horas), leitura no DRX (~15 minutos), correções e interpretações no difratograma (~10 minutos), obtenção da relação Gt/(Gt+Hm) (~3 minutos), teor de ferro extraído por ditionito-citrato bicarbonato (Fe_d) e ferro extraído por oxalato de amônio (Fe_o) (~7 horas) e, finalmente, leitura do conteúdo de Hm e Gt por DRX (~2 minutos). Enquanto para o procedimento por ER com a primeira e segunda derivada da função Kubelka-Munk, levou-se em torno de 7 horas e 25 minutos, com: leitura no espectrômetro, aplicação das derivadas na função Kubelka-Munk e cálculo das amplitudes das bandas espectrais (~23 minutos), Fe_d e Fe_o (~7 horas) e, por fim, leitura do conteúdo de Hm e Gt por ER (~2 minutos), alcançando um R^2 de 0,99 de validação para essa estimativa dos óxidos de ferro, em relação ao DRX. Nota-se que a análise de DRX é mais trabalhosa, precisando de vários reagentes, enquanto, por ER, a análise é indireta e alcança resultados ótimos. Com isso, pode-se dizer que a análise DRX por ser dispendiosa, limita-se em fazer poucas amostras pelo tempo que leva e pelo dinheiro investido, tornando-se difícil realizar análises de grande número de amostras de uma região, que pode ser de suma importância para gerar um banco de dados de mineralogia.

Apesar dessas limitações, essa análise não pode ser substituída, mas sim complementada pelas análises de espectroscopia de refletância, dando suporte na quantificação dos teores dos minerais. Além disso, pode ser realizada uma análise qualitativa da mineralogia do solo através da espectroscopia, proposta essa não muito estudada, que teria como foco a identificação da composição mineralógica do solo, com isso, sendo capaz de realizar uma rápida interpretação do solo.

3. CAPÍTULO II – PREDICTION OF SOIL TEXTURE CLASSES THROUGH DIFFERENT WAVELENGTH REGIONS OF REFLECTANCE SPECTROSCOPY AT VARIOUS SOIL DEPTHS[2]

3.1. Introduction

Soil granulometry aims to characterize the soil body in terms of particles, i.e. at pre-defined size categories of different ranges. The most commonly used size categories, also adopted by World Reference Base (WRB) for soil resources (FAO, 2015) are clay, silt and sand, with corresponding size ranges of 0 - 0.002, 0.002 - 0.05 and 0.05 - 2 mm, respectively. Soil texture has a crucial implication in physical, chemical and biological characteristics of the soil, thereby strongly influencing its other key properties such as soil structure, water and thermal regime, accessibility of plant available nutrients, living organism diversity, plant growth, as well as soil quality in general. Thus, its determination and mapping play an important role in land use planning, water regime and soil protection measurements (KLEIN et al., 2010; TÜMSAVAŞ et al., 2018).

Routine laboratory analyses determine soil texture on standard methods such as hydrometer or pipette method (TEIXEIRA et al., 2017), that are costly and time-consuming, and today not suitable for a large number of soil samples and high-resolution mapping. At present, the demand for accurate and low-cost soil information is growing due to the demands of precision agriculture and land use planning. Therefore, there is a need for new, faster and cheaper methodology (PENG et al., 2014; SORIANO-DISLA et al., 2014; ZHAO et al., 2018).

[2] Adapted from article published in *Catena Journal* (doi.org/10.1016/j.catena.2020.104485).

The advantages of soil spectroscopy analyses include, in particular, rapidness, economic convenience, non-destructive application and freeing from chemical agents involved. Furthermore, many measurements can be made in a short period of time, allowing a large amount of soil information to be collected quickly (VISCARRA ROSSEL et al., 2006; WANG et al., 2014; ZHU; WEINDORF; ZHANG, 2011). Besides that, with only one soil sample measurement a variety of soil properties can be determined at once (MOHANTY; GUPTA; DAS, 2016; WIGHT; ASHWORTH; ALLEN, 2016; ZHANG et al., 2017). These are the reasons for success of proximal soil sensing techniques in visible (VIS), near-infrared (NIR), shortwave-Infrared (SWIR) and mid-infrared (MIR) regions.

Reflectance spectroscopy uses electromagnetic energy to analyze the behavior of an object. Energy interacts with the object in two ways: part of the energy is absorbed and part of it is reflected. The absorption characteristics that occur in the spectral curve due to contact with some components are due to the electronic and vibration process. In the electronic process, the transitions between the energy levels of atomic orbitals are responsible for the absorption characteristics in the spectra. These processes occur mainly in the visible spectral region and near infrared. The vibrational process, which occurs due to vibrations of the molecular bonds resulting from energy absorption, occurs predominantly in infrared regions such as shortwave infrared and mid-infrared. As each soil has different constitutions, the respective spectra will have different absorption characteristics (BOWERS; HANKS, 1965; HUNT; SALISBURY, 1970).

At VIS range of the soil spectrum (350-700 nm) exhibit absorption features related to iron oxides (e.g., hematite and goethite) (VISCARRA ROSSEL; BEHRENS, 2010; SORIANO-DISLA et al., 2014), whereas within the NIR-SWIR region (700-2500 nm) absorption features of organic matter, carbonates, water features and clay minerals (e.g., kaolinite, smectite and illite) can be detected (OMRAN, 2017; VISCARRA ROSSEL et al., 2006; ZHAO et al., 2018). In addition, at MIR region (2500 to 25000 nm / 4000-400 cm^{-1}) absorption features of clay minerals, quartz, iron oxides and organic matter occur (VISCARRA ROSSEL et al., 2006; WANG et al., 2014).

On top of that, many studies are being conducted using reflectance spectroscopy techniques to estimate various soil properties that have distinct

spectral features, such as soil organic carbon (VISCARRA ROSSEL et al., 2006; CAMBOU et al., 2016; VAŠÁT et al., 2017a), iron oxides (SELLITTO et al., 2009; VISCARRA ROSSEL; BEHRENS, 2010), moisture content (WIGHT; ASHWORTH; ALLEN, 2016), quantification of mineral contents (RAMAROSON et al., 2017) and silicon concentration (LANDRÉ et al., 2018). In addition, other soil properties can also be indirectly predicted based on their relationship to those with direct spectral response, such as clay content (PENG et al., 2014; TÜMSAVAŞ et al., 2018), estimation of root density (XU et al., 2017), estimation of arsenic content in soils (SHI et al., 2016), soil total nitrogen (MORELLOS et al., 2016), organic matter (NANNI; DEMATTÊ, 2006; ZHENG et al., 2016). Previous studies utilized a large spectral range (from VIS to MIR) and different statistical methods to predict particle size fractions. For example, several authors carried out studies in VIS-NIR region to predict soil texture classes, using partial least-squares regression (PLSR), Cubist regression and support vector regression (SVR) (DUDA et al., 2017; TÜMSAVAŞ et al., 2018; VASAVA et al., 2019; ZHANG et al., 2017). Wijewardane et al. (2018) estimated soil texture fractions with spectroscopy in MIR region using PLSR and artificial neural networks (ANN). Minasny et al. (2009) also estimated soil particle size in the MIR region, however using the Cubist algorithm. Madari et al. (2006), used from NIR to MIR region with PLSR to predict various soil properties, including particle size. Viscarra Rossel et al. (2006) used the VIS-NIR-SWIR and MIR region with the PLSR algorithm for predicting particle size. Furthermore, previous studies have used some sort of spectral data pre-processing, such as first and second derivative, continuum removal, PCA, SNV, Savitzky-Golay filter, with the objective of improving prediction results, however increasing spectral processing.

Moreover, most studies do not consider the soil depths in the models. It is known that topsoil usually has more organic matter, which differs from the deeper layers (JIANG et al., 2017). Furthermore, along the profile, soil properties such as mineralogy and texture vary, and this aspect has been little explored by the methods of spectroscopy, being able to influence in the prediction models. Therefore, it is necessary to evaluate models for each depth to verify the influence on the calibration for soil texture prediction.

Thereby, it is promising that reliable predictions can be found using the VIS-NIR-SWIR and MIR spectral regions without pre-processing of the spectra

(raw spectra), to emphasize the differences between these two spectral regions and reduce data processing demands at same time. Thus, the objective of this study was to: a) explore the possibilities of prediction of the content of three fraction contents (clay, sand and silt) in subtropical soils; b) compare the accuracy of predictive models calibrated on different spectral regions (VIS-SWIR-NIR and MIR); c) assess the effect of different soil depths on predictions, and finally d) explain the differences in prediction accuracy in the means of the input data structure, as this aspect is rarely addressed in the literature.

3.2. Materials and methods

3.2.1. Study area and soil sampling

The study was conducted in the state of Rio Grande do Sul, southern Brazil, in a reforestation area of 325 hectares (Fig. 1). According to the Köppen classification system, the regional climate is the Cfa - humid subtropical climate, with an annual average rainfall of 1400 mm and the average temperature of the coldest month between 0 °C and 18 °C and the hottest month above 22 °C (WREGE et al., 2012). Igneous rocks (monzogranite, sienogranite) and alluvial deposits (sand, gravel) characterize the parent material of the study area. The soils found in the area were Rhodic Acrisol, Xanthic Alisol, Xanthic Acrisol and Dystric Regosol. The Alisol and Acrisol have a textural B horizon below A and E with low clay activity or high activity with low base saturation. However, the Regosols are soils poorly developed with base saturation < 50%, have no lithic contact up to 50 cm depth, assuming the B horizon at the beginning of the formation, according to Brazilian Agricultural Research Corporation and World Reference Base for Soil Resources (EMBRAPA, 2013; IUSS Working Group WRB, 2015). Therefore, the soil type varies from very clayey to sandy soils, with clay content varying from 5 to 70%, sand between 14 and 86% and silt from 9 to 42% (Table 1).

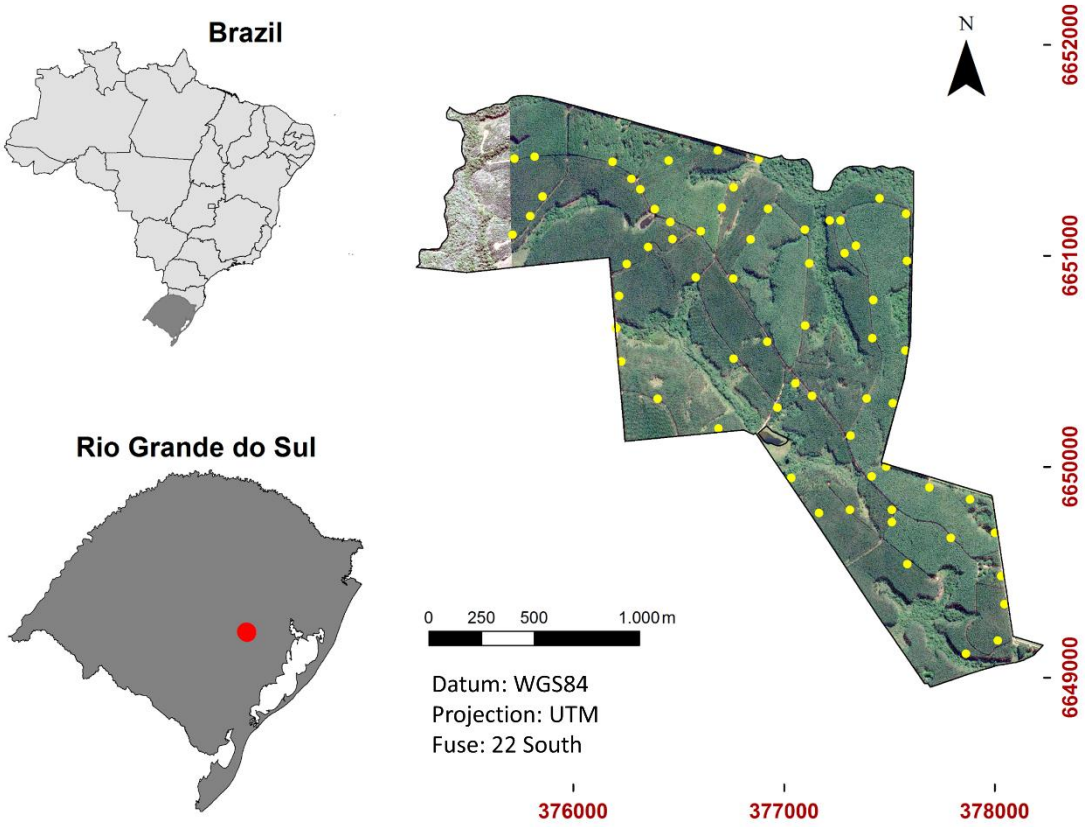

Fig. 1. Location of the study area in the state of Rio Grande do Sul, Brazil, with 66 soil point observations.

A total of 197 samples were collected at depths of 0-20, 20-40 and 40-60 cm at 66 sampling locations (one soil site had a depth of approximately 50 cm, so only the first two layers were collected), being 42 samples on the Xanthic Alisol, 44 on Rhodic Acrisol, 27 on Xanthic Acrisol and 84 on Dystric Regosol. The soil samples were air-dried, then milled and sieved. Fractions smaller than 2 mm were used in both soil granulometry and spectroscopy (VIS-NIR-SWIR) analysis. For MIR analysis, less than 1 cm^3 of sample is placed in the container for scanning, because of that the soil samples were ground and sieved to 0.149 mm. With the reduction in size, the incident ray will easily penetrate between the particles, improving the interaction between them, avoiding specular reflection and increasing diffuse reflection, allowing a more representative analysis of the sample (LE GUILLOU et al., 2015). The particle size fractions of clay, silt, and sand were determined using the Pipette method with NaOH dispersant according to the standard soil analysis method (TEIXEIRA et al., 2017).

Divided by the three different soil depths, it is evident that the deeper, the greater the variability of soil texture fractions content. The trend of increasing variability with the soil depth was observed for all three texture fractions, i.e. clay, sand and silt (Table 1), while the most pronounced was for clay and the less for the silt fraction.

Table 1. Descriptive statistics of soil properties of the total dataset and dataset separated by the three soil depths (197 soil samples).

Depth (cm)	***Number of samples***	***Minimum***	***Maximum***	***Mean***	***Median***	***Standard deviation***	***Skewness***	***Kurtosis***
				Clay (%)				
0-20	*66*	*5.2*	*45.6*	*22.1*	*20.2*	*8.5*	*0.98*	*4.04*
20-40	*66*	*10.5*	*66.5*	*30.5*	*27.1*	*13.5*	*0.84*	*2.97*
40-60	*65*	*10.7*	*70.5*	*41.3*	*39*	*15.6*	*0.19*	*1.96*
all depth	*197*	*5.2*	*70.5*	*31.3*	*30*	*15*	*0.83*	*2.81*
				Sand (%)				
0-20	*66*	*33.7*	*86.1*	*59.4*	*60.8*	*9.9*	*-0.39*	*3.68*
20-40	*66*	*16.5*	*72.9*	*50.3*	*53.8*	*13.2*	*-0.58*	*2.68*
40-60	*65*	*13.7*	*73.0*	*39.8*	*40.1*	*14.1*	*0.15*	*2.31*
all depth	*197*	*13.7*	*86.1*	*50*	*52.7*	*14.8*	*-0.45*	*2.49*
				Silt (%)				
0-20	*66*	*8.6*	*32.5*	*18.5*	*18.4*	*4.6*	*0.28*	*3.31*
20-40	*66*	*11.5*	*35.9*	*19.1*	*18.6*	*4.7*	*0.97*	*4.51*
40-60	*65*	*8.9*	*41.7*	*18.9*	*18.5*	*5.4*	*1.4*	*7.42*
all depth	*197*	*8.6*	*41.7*	*18.8*	*18.5*	*4.9*	*0.97*	*5.56*

3.2.2. Soil spectra collection

Soil reflectance data in VIS-NIR-SWIR region were obtained with FieldSpec Pro spectrometer (Analytical Spectral Devices, Bouder, Colorado, USA) with spectral resolution interpolated to 1 nm for wavelengths of 350 to 2500 nm. Before scanning the soil spectra, soil samples were placed in petri dishes (9 cm diameter by 1.5 cm height) and were homogeneously distributed to reduce the influence of roughness of the material. The spectral sensor captured the light through a fiber-optic cable, allocated at 8 cm from the sample surface. The sensor scanned an area of approximately 2 cm^2 at the center of the sample. Two 50-W

halogen lamps were used as a light source, generating non-collimated rays to the target plane. The lamps were placed 35 cm from the sample and at an angle of 30° zenith. The instrument was calibrated using a Spectralon standard white plate and this procedure was performed at the beginning and repeated every 20 minutes during readings. For each soil sample, the spectroradiometer device automatically calculated an average of 100 scans. On top of that, three independent measurements were taken for each soil sample, rotating the Petri dish by 90° to assure a better representation of the surface area examined. The final spectrum was finally calculated as an average value of the three spectra scans. Geometry and data acquisition were obtained according to Terra et al. (2015). The VIS-NIR-SWIR spectra presented offset at 1100 and 1830 nm and were removed using the *spliceCorrection* function in the *prospectr* package (STEVENS; RAMIREZ-LOPEZ, 2014) in R software (R CORE TEAM, 2019). This function corrected the steps in the input spectral matrix by linear interpolation.

The reflectance spectra in MIR region (4000-400 cm^{-1} / 2500- 25000 nm) were obtained by Alpha Sample Compartment RT (Bruker Optik GmbH) device equipped with a diffuse reflectance acquisition accessory (Drift). The spectra were acquired with a resolution of 2 cm^{-1} and 32 scans per spectrum. Less than 1 cm^3 of sample was placed in the container of the equipment for scanning. Before each individual soil sample scanning, the reference spectrum was obtained by calibrating the sensor. A gold plate was used as a reference to remove radiation interference from the sample spectrum.

3.2.3. Predictive modeling and validation

Predictive models for the three soil texture fractions were calibrated firstly for a total dataset with all three soil depths merged, and secondly separately for each of the three soil depths, in order to analyze relations between prediction accuracy indices and data structure. For validation purposes (independent validation), all data sets were randomly separated in calibration samples (70%) and validation samples (30%). Cubist regression algorithm (KUHN; QUINLAN, 2018) in R software (R CORE TEAM, 2019) was applied to train predictive models

for clay, sand and silt content in three separate modeling approaches differing in spectral region: i) VIS-NIR-SWIR, ii) MIR and iii) VIS-NIR-SWIR plus MIR.

The Cubist model, introduced to soil modeling by Minasny and McBratney (2008), is an alternative method for handling soil spectra, that is known for high accuracy estimates, convenient interpretation of the model structure and variable selection (HENAKA ARACHCHI; FIELD; MCBRATNEY, 2016). In order to improve the Cubist model, two parameters were adjusted: the set of models called "committees", to improve the prediction of the models and the number of neighboring observations (neighbors), to adjust the forecast of the rules. The values for the parameter "committees" were 1 and 100. The ideal number for "neighbors" were 0 and 9, varying according to the data set analyzed.

To assess the performance of predictive models, three accuracy indices, i.e. coefficient of determination (R^2), root mean square error (RMSE) and ratio of performance to inter-quartile (RPIQ), were applied. The R^2 range from 0 to 1, with 1 being the optimal value, that is, all the variance of the response variable was explained by the model. The RMSE has the same data units as the analyzed attributes and has the role of measuring the overall accuracy of the model prediction. The closer to zero, the better the prediction of the model. RPIQ value were used to evaluate the quality of the models, considering the reliability of the prediction: RPIQ > 2,0: excellent models; 1,40 < RPIQ < 2,0: reasonable models; RPIQ < 1,4: untrusted models (CHANG et al., 2001; CHANG; LAIRD, 2002; TERRA, 2011). We considered the best model to be the one with the highest values of R^2 and RPIQ combined with lower values of RMSE.

3.3. Results and discussion

3.3.1. Soil texture variation

The soils vary from very clayey to sandy soils, with clay content ranging from 5.2 to 70.5% and an average value of 31.26% at all depths, sand has an average value of 49.9% and minimum value of 13.7% and maximum of 86.1 and silt ranges from 8.6 to 46.7% with an average of 18.84% at all depths. Frequency

distribution of the three fractions (clay, silt and sand) differs from case to case (Fig. 2).

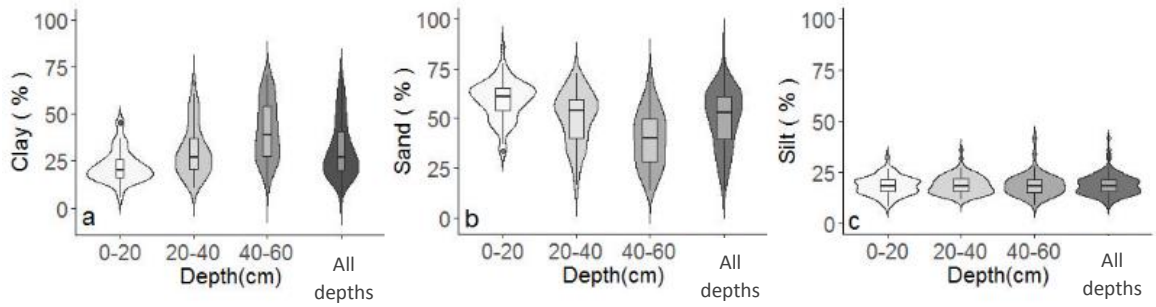

Fig. 2. Frequency distribution and variability of three soil particle size fractions, i.e. clay, sand and silt, for the three different soil depths, i.e. a) 0-20 (66 samples), b) 20-40 (66 samples) and c) 40-60 cm (65 samples) and for total content (all depths).

It is skewed largely for clay (right skewed) and sand (left skewed), while it is not skewed noticeably for silt, but bimodal in that case. At the depth 40-60 cm, the clay and sand fractions are distributed more uniformly. Among the three fractions, the shortest range of values (the lower variability) applies to silt fraction. Concerning the changes in soil texture distribution with soil depth, the content of clay increases, sand does the opposite, and silt fraction does not change noticeably.

3.3.2. Description of spectral curves

Three features in a spectral curve should be observed for visual analysis, reflectance intensity (albedo), absorption features and spectral shape (DEMATTÊ, 2002). The shape of the spectral curve is influenced by the physical and chemical properties of the soil, altering the albedo and absorption features. In general, for all regions (VIS-NIR-SWIR and MIR), variations in albedo refer mainly to influence of particles size, sandy soils tend to have higher reflectance intensity and positive curve angles, and clay soils tend to have lower reflectance intensity, however, with more pronounced absorption features (DEMATTÊ et al., 2014).

In the VIS-NIR-SWIR region, in the 450 to 520 nm range, iron oxides (hematite and goethite) can be identified by absorption features, and at 450 nm goethite forms a specific shoulder in the spectral curve (Fig. 3) (DEMATTÊ et al., 2014). There is another absorption feature in the bands 1410 and 1920 nm, which refer to OH^- and H_2O stretching vibration of clay minerals, which is visually identified by large absorptions with 'V' shape (ZHAO et al., 2017). In the range of approximately 2200 nm the absorption features are due to the clay minerals (XU et al., 2017; YU; HUNT, 2018), within this absorption a specific small shoulder can be identified at 2160 nm, which refer to the presence of kaolinite (Fig. 3) (DEMATTÊ et al., 2014).

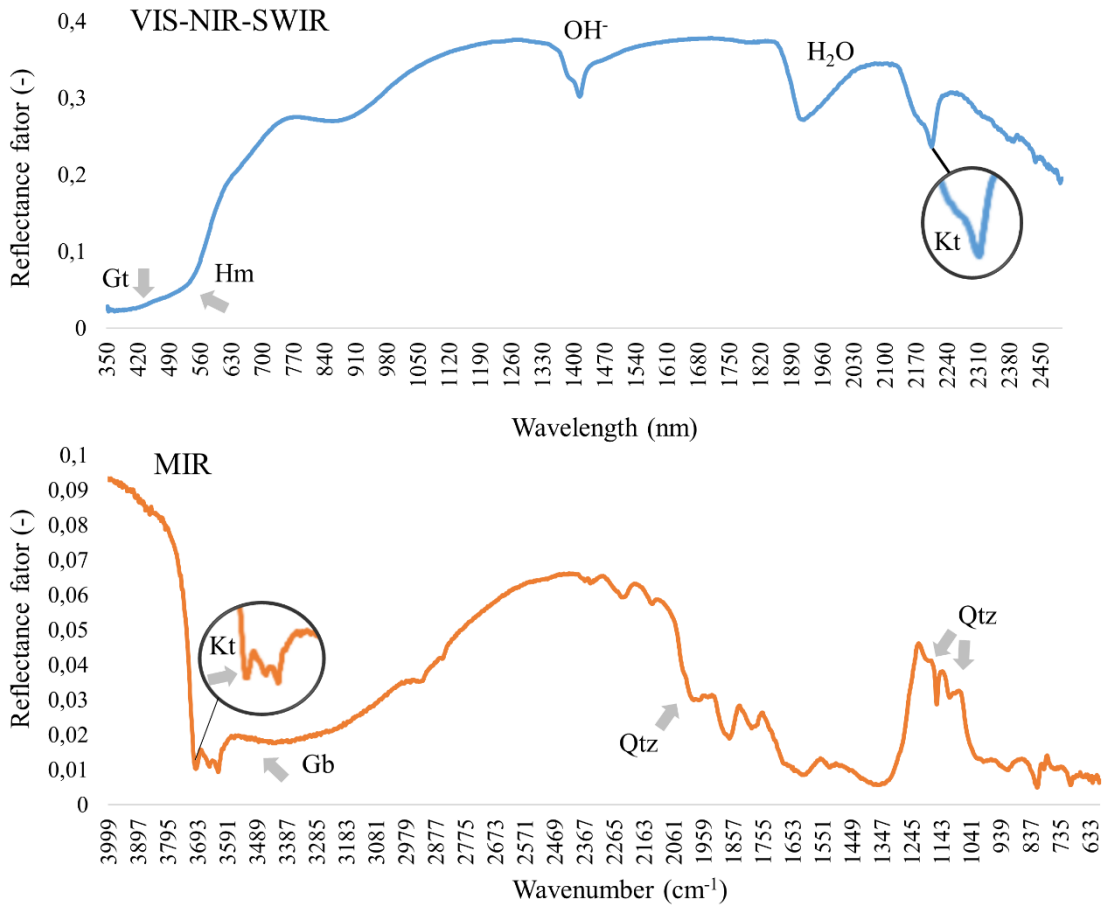

Fig. 3. Some features of soil properties that influence the shape of the spectra for the VIS-NIR-SWIR and MIR raw spectra. Gt: Goethite, Hm: Hematite, Gb: Gibbsite, Kt: Kaolinite, Qtz: Quartz, OH^- and H_2O: O-H stretching and O–H stretching of H-bonded water.

MIR region is strongly influenced by quartz and clay minerals. Absorption features and peaks of reflectance around 3500 to 3700 cm^{-1} refer to kaolinite and gibbsite due to the O-H stretching vibration of kaolinite and gibbsite group (Fig. 3) (NGUYEN et al., 1991; NAYAK; SINGH, 2007). Another mineral exposed in the MIR region is quartz, presenting absorption features at ~2000 cm^{-1}, ~1180 cm^{-1} and approximately at 1100 cm^{-1}, which influences in spectral curve with greater reflectance intensity (Fig. 3) (SALISBURY; D'ARIA, 1992).

3.3.3. Model combining all soil depths

For clay fraction, the calibrated Cubist models presented a reliable prediction accuracy, with associated R^2 values ranging from 0.89 to 0.94, RMSE from 3.6 to 5.1% and RPIQ from 4.47 to 6.26 (Table 2). For sand, the values varied from 0.81 to 0.88 for R^2, RMSE from 5.1 to 6.5% and RPIQ from 3.17 to 4.05, implying that the prediction models also present high quality. The predictive models of silt presented poor quality, with values of R^2 going from 0.06 to 0.18, RMSE from 4.0 to 4.1% and RPIQ from 1.49 to 1.53 (Table 2). The prediction performance for clay and sand was more accurate than that obtained for silt, following the same trend observed in other studies (TÜMSAVAŞ et al., 2018; VISCARRA ROSSEL et al., 2006; ZHANG et al., 2017). The low performance for silt prediction can be explained by the error associated with the standard method (MADARI et al., 2006; PINHEIRO et al., 2017), where the silt is calculated indirectly, by the difference in total soil mass, which means that the largest part of the analytical error is propagated in the silt fraction.

For clay content, the R^2 obtained in the VIS-NIR-SWIR, MIR and VIS-NIR-SWIR-MIR were very high with a low RMSE. For VIS-NIR-SWIR model, the results were R^2 of 0.92 for calibration and 0.89 for validation with RMSE of 5.1% (Table 2), better than Camargo et al. (2015), who used the PLSR for one-hundred surface soil samples at different geomorphic surfaces, where they found an R^2 of 0.70 for validation. Zhang et al. (2017) used the cubist algorithm in data set with clay content ranging from 3 to 88%, found an R^2 of 0.64 for calibration and 0.70 for validation, with RMSE of 14.7% for validation. More recently, using 543 surface soil samples from agricultural fields at different soils, with an average clay

content of 26.5%, Vasava et al. (2019) also performed clay prediction using PLSR, finding R^2 of 0.73 with RMSE of 5.40% for validation, with results with less accuracy compared to this study. For the prediction of the sand content, the results were also significant in the VIS-NIR-SWIR, we achieved the R^2 of 0.87 and RMSE of 5.4% for calibration and R^2 of 0.81 and RMSE of 6.5% for validation (Table 2). Zhang et al. (2017) used the same Cubist algorithm and obtained R^2 of 0.73 and RMSE of 1.3% for calibration and R^2 of 0.5 and RMSE of 1.8% for validation, with sand content ranging from 0.05 to 90%. O'Rouke et al. (2016), with two datasets at different depths and soils, using Cubist, found R^2 of 0.35, and using variance weighted averaging (VWA) found R^2 of 0.85 and RMSE of 0.7% for validation, reaching better accuracy. With 300 surface soil samples from three catenas where the sand content ranged from 0.3 to 36.9%, Duda et al. (2017) predicted sand content using support vector regression (SVR) and reached R^2 of 0.18 and RMSE of 5.5% for validation. Vasava et al. (2019) obtained R^2 of 0.80 with RMSE of 3.28% using PLSR for calibration of the model, which showed similar accuracy compared to this study. Tümsavaş et al. (2018), with sand content ranging from 12 to 55%, found R^2 of 0.81 and RMSE of 3.84% for predicting sand content by PLSR analysis, resulting in better accuracy. Figure 4 shows the validation results for all models.

Table 2. Performances of the models for the soil properties applying Cubist algorithm through reflectance spectroscopy in different spectral regions.

		Calibration			***Validation***		
Soil Properties	***Spectral region***	R^2_{cal}	$RMSE_{cal}$ (%)	$RPIQ_{cal}$	R^2_{val}	$RMSE_{val}$ (%)	$RPIQ_{val}$
Clay	*VIS-NIR-SWIR*	*0.92*	*4.2*	*4.59*	*0.89*	*5.1*	*4.47*
	MIR	*0.96*	*2.9*	*6.79*	*0.94*	*3.7*	*6.18*
	VIS-NIR-SWIR-MIR	*0.97*	*2.7*	*7.27*	*0.94*	*3.6*	*6.26*
Sand	*VIS-NIR-SWIR*	*0.87*	*5.4*	*4.12*	*0.81*	*6.5*	*3.17*
	MIR	*0.96*	*3.2*	*7.00*	*0.88*	*5.1*	*4.05*
	VIS-NIR-SWIR-MIR	*0.96*	*3.1*	*7.12*	*0.88*	*5.1*	*4.03*
Silt	*VIS-NIR-SWIR*	*0.61*	*3.4*	*1.86*	*0.06*	*4.1*	*1.49*
	MIR	*0.66*	*3.0*	*2.14*	*0.18*	*4.0*	*1.53*
	VIS-NIR-SWIR-MIR	*0.71*	*2.8*	*2.3*	*0.14*	*4.1*	*1.49*

For the MIR model, the prediction of the clay content obtained excellent results, with R^2 of 0.96 and RMSE of 2.9% for calibration, and R^2 of 0.94 with RMSE of 3.7 % for validation (Fig. 4). Wijewardane et al. (2018), in a study with a MIR spectral library of 20,153 soil samples and clay content ranging from 21 to 96%, performed prediction of clay using the MIR with PLSR and ANN for model calibration and achieved R^2 results of 0.85 and 0.77 with RMSE of 6% and 7.6%, comparatively worse than the results found in this study. The same occurs in McCarty and Reeves (2006), using a data set of 544 soil samples at two depths (0-10 cm and 10-30 cm) and clay content ranging from 11 to 29%, where they found R^2 of 0.87 with RMSE of 1.2%, and R^2 of 0.84 with RMSE of 1.3%, for calibration and validation, respectively. Minasny et al. (2009) found R^2 with values ranging from 0.86 to 0.94 for calibration and from 0.79 to 0.86 for validation, also using the cubist algorithm in a study with 1931 soil samples subdivided into different areas. In addition to those studies already mentioned, the present study reached higher prediction accuracy for clay content than others applying different pre-processing and modeling techniques (D'ACQUI; PUCCI; JANIK, 2010; JANIK; FORRESTER; RAWSON, 2009; JANIK; SKJEMSTAD; MERRY, 1998; MADARI et al., 2006; PENG et al., 2014; VISCARRA ROSSEL et al., 2006).

For the prediction of sand content with MIR, we found an R^2 of 0.96 with RMSE of 3.2% and R^2 of 0.88 and RMSE of 5.1%, for calibration and validation, respectively (Fig. 4). Minasny et al. (2009), using the Cubist algorithm for model calibration, found R^2 ranging from 0.79 to 0.85 for validation. The same occur with Wijewardane et al. (2018), where they reached R^2 of 0.83 and RMSE of 12% for validation, with sand content ranging from 0.2% to 100%. For the combined model (VIS-NIR-SWIR-MIR), were found similar results to the MIR model (Fig. 4).

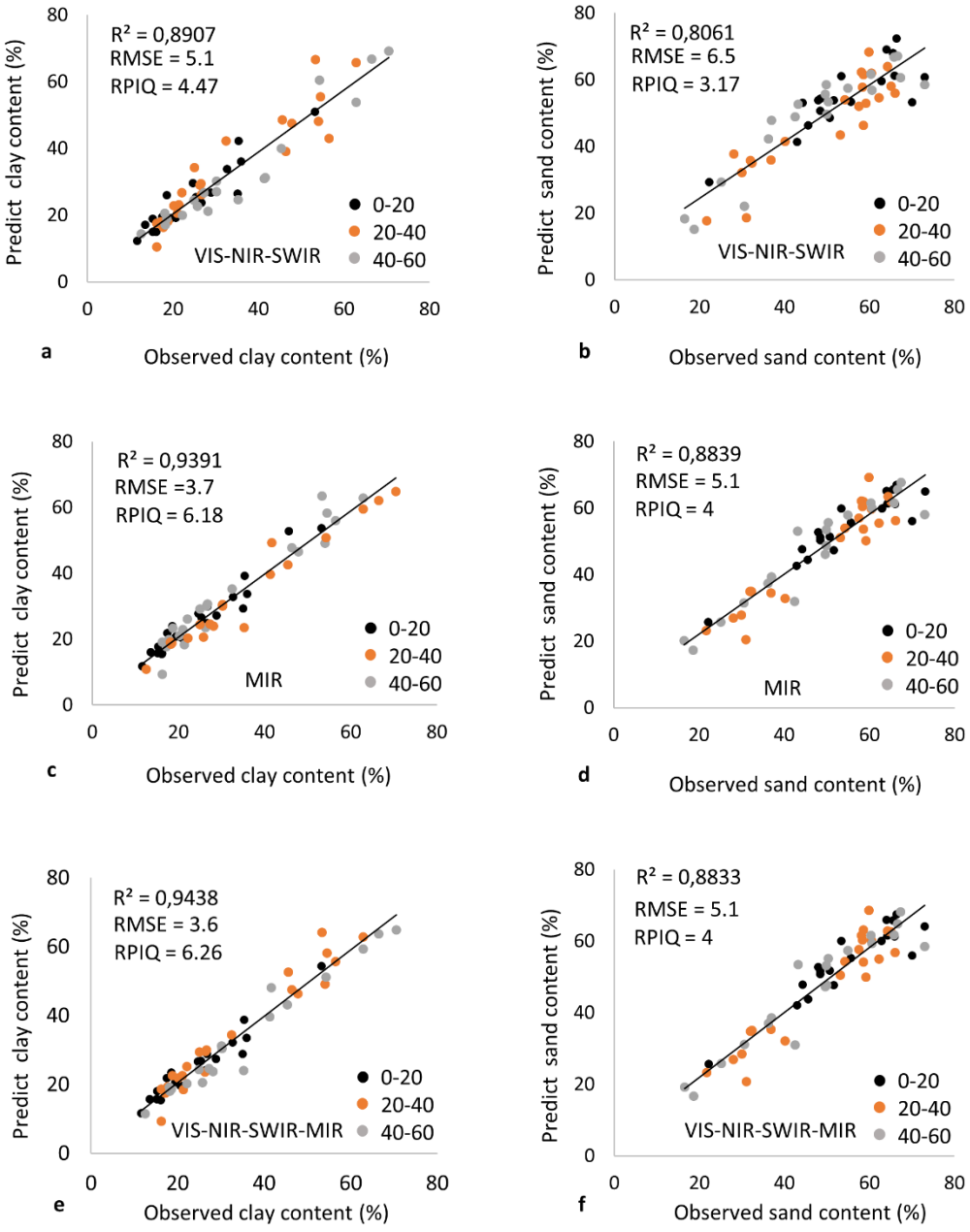

Fig. 4. Results of validation of clay and sand prediction under the VIS-NIR-SWIR (a, b), MIR (c, d) and VIS-NIR-SWIR-MIR (e, f) models, respectively.

According to Soriano-Disla et al. (2014), the MIR region has much more spectral information in contrast to VIS-NIR-SWIR and also better soil correlated peaks. The MIR spectral region contains distinct peaks related to specific soil properties, which is easily observed in the spectra, where in the VIS-NIR-SWIR region this detection is more complex. MIR spectrometers require finer milling of the samples, needing more sample preparation, however, the predictions tended

to be more accurate (LANDRÉ et al., 2018). Figure 5 shows the ternary plot of the observed values compared to the VIS-NIR-SWIR and MIR models.

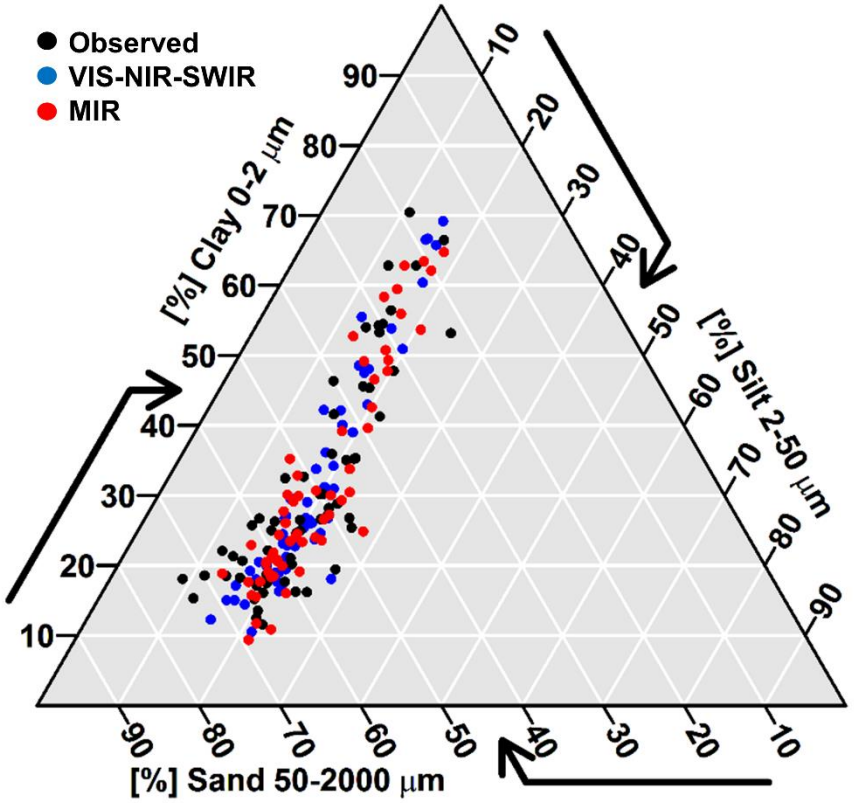

Fig. 5. Soil texture of the observed and predicted values (VIS-NIR-SWIR and MIR) of validation set.

The VIS-NIR-SWIR, MIR and combined VIS-NIR-SWIR-MIR were not able to predict silt with high accuracy differently from clay and sand content.

3.3.4. Dataset separated by soil depth

Separate calibration for the three soil depths revealed a distinct difference in prediction accuracy for all tested soil texture fractions (Table 3). However, the spectral region also plays an important role. Depending on the spectral region, the best accuracy achieved vary between the soil depths from case to case. For clay content, the most accurate results at VIS-NIR-SWIR region were achieved for soil depth 20-40 cm (RMSE of 5.6%), for MIR region, it was 0-20 (3.5%) and

for combination of all spectral regions it was 40-60 cm (3.6%). In the MIR region (the highest accuracy among all regions), the achieved results in terms of RMSE for clay content were 3.5, 6.1 and 4.9% for layers 0-20, 20-40 and 40-60, respectively.

On the other hand, for sand content, the most accurate results were obtained for the depth 0-20 cm, regardless the spectra region, indicating that the soil depth is stronger factor than the spectral region in this case. For sand, the prediction accuracy was similar for all spectral regions, as it was 5.5, 5.4 and 5.6% (RMSE) for VIS-NIR-SWIR, MIR, and combination, respectively. It is believed that the best clay accuracy was found in the subsurface and to sand in the surface due to the higher content of the respective fractions at these soil layers. The clay fraction having higher contents in depths of 20-40 and 40-60 cm and the sand fraction was measured as having higher contents in samples depths of 0 to 20 cm. Finally, for silt content no reliable prediction was achieved for any of the three depths, as was not the case for total dataset either (Table 2).

The variability of the input data has a clear impact on the final prediction accuracy expressed with R^2, RMSE and RPIQ (Table 3). This is particularly apparent for clay and sand fractions for which the variation among the three soil depths vary largely. From the accuracy assessment point of view, as the prediction accuracy in terms of R^2 increases (towards more accurate predictions) with increasing variation of the data, the RMSE however, increased (meaning worse prediction accuracy) confirming findings previously reported by Vašát et al. (2017b). In other words, larger range of values in the input dataset leads to most accurate results in terms of R^2, but contradictorily to less accurate prediction in terms of RMSE, at the same time. This means that variation of the input data should be taken into account when interpreting the results, but more importantly, if applicable, it should take into account comparison of results between different studies.

Table 3. Performances of the models for the soil properties applying Cubist algorithm of 197 soil samples divided by three depths through reflectance spectroscopy in different spectral regions.

			Calibration			Validation		
Spectral region	**Soil Properties**	**Depths (cm)**	**R^2_{cal}**	**$RMSE_{cal}$ (%)**	**$RPIQ_{cal}$**	**R^2_{val}**	**$RMSE_{val}$ (%)**	**$RPIQ_{val}$**
VIS-NIR-SWIR	*Clay*	*0-20*	*0.80*	***3.7***	*2.29*	*0.68*	*5.6*	*1.93*
		20-40	*0.81*	*5.8*	*3.08*	***0.84***	***5.6***	*2.47*
		40-60	***0.93***	*4.3*	***6.30***	*0.77*	*6.9*	***3.07***
	Sand	*0-20*	*0.40*	*7.4*	*1.34*	***0.74***	***5.5***	***2.36***
		20-40	***0.81***	***5.6***	*3.05*	*0.57*	*10*	*1.85*
		40-60	***0.81***	*6.6*	***3.34***	*0.55*	*9.5*	*1.61*
	Silt	*0-20*	*0.09*	*5.2*	*1.37*	*0.12*	***2.9***	*1.52*
		20-40	***0.62***	***3.0***	***1.98***	***0.21***	*4.0*	***1.63***
		40-60	*0.09*	*4.7*	*1.27*	*0.10*	*6.1*	*0.99*
MIR	*Clay*	*0-20*	*0.85*	*3.1*	*2.71*	*0.88*	***3.5***	*3.07*
		20-40	*0.95*	*3.1*	*5.73*	*0.81*	*6.1*	*2.26*
		40-60	***0.97***	***3.0***	***8.95***	***0.91***	*4.9*	***4.37***
	Sand	*0-20*	***0.88***	***3.4***	*2.89*	*0.74*	***5.4***	*2.39*
		20-40	*0.76*	*6.3*	*2.71*	*0.57*	*9.2*	*2.01*
		40-60	*0.82*	*6.3*	***3.46***	***0.76***	*6.0*	***2.58***
	Silt	*0-20*	***0.66***	***3.0***	***2.30***	*0.01*	***3.8***	*1.17*
		20-40	*0.28*	*4.0*	*1.48*	***0.30***	*3.8*	***1.71***
		40-60	*0.39*	*3.8*	*1.55*	*0.23*	*5.6*	*1.09*
VIS-NIR-SWIR-MIR	*Clay*	*0-20*	*0.91*	***2.5***	*3.42*	*0.88*	*4.1*	*2.66*
		20-40	*0.96*	*2.7*	***6.70***	*0.80*	*6.2*	*2.23*
		40-60	***0.98***	*2.5*	*1.09*	***0.93***	***3.6***	***5.88***
	Sand	*0-20*	*0.89*	***3.2***	*3.07*	*0.74*	***5.6***	*2.33*
		20-40	***0.94***	*3.3*	***5.11***	***0.80***	*6.5*	***2.86***
		40-60	*0.86*	*5.4*	*4.04*	*0.67*	*7.0*	*2.21*
	Silt	*0-20*	***0.67***	*3.0*	***2.34***	*0.03*	*3.8*	*1.16*
		20-40	*0.59*	***3.2***	*1.88*	***0.41***	***3.4***	***1.93***
		40-60	*0.63*	*3.0*	*1.99*	*0.07*	*9.1*	*0.67*

As also found by observed vs. predicted scatter plots (Fig. 5) by merging the data from all three soil depths, the correlation clouds become narrower than they would be in the case of separate datasets, resulting in larger R^2 values. Such

trend was not apparent in the case of silt content, where the data are distributed more uniformly across all three soil depths (Fig. 2).

3.3.5. Variable importance

Figures 6 and 7 showed the VIS-NIR-SWIR and MIR wavelengths and wavenumbers which were most important for the prediction of clay and sand content. For the VIS-NIR-SWIR spectra, the bands of high importance for the clay prediction were found in several regions of the spectrum, such as 525 and 875 nm, which are associated with the hematite absorption bands (FANG et al., 2018). Absorption at 620 and 680 nm, which correspond to color information was correlated with clay minerals (GOMEZ; LAGACHERIE; COULOUMA, 2008). Another important peak of the spectrum was at 1410 nm, which can be attributed to the kaolinite group and the OH^- stretching vibration. The 1920 nm peak also showed great importance referring H-O-H bending in structural/adsorbed H_2O (ZHAO et al., 2017). The clay pattern associated with Al-OH absorption was found in 2200nm (XU et al., 2017; YU; HUNT, 2018). In addition, the same peaks at 1410, 1910 and 2200 nm were characterized as being kaolinite and illite absorption bands. The absorption peak at Al-OH at 2200 nm is characteristic of both kaolinite and illite (CAMARGO et al., 2018; DEMATTÊ et al., 2006; ZHAO et al., 2017), but the specific small shoulder that refers to the presence of kaolinite has been identified in 2165 nm (DEMATTÊ et al., 2014). Moreover, the peak at 2480 nm was one of the most important variables for the clay model, being associated with the presence of Fe-OH (FANG et al., 2018).

For the prediction model of sand, the most important peaks in the VIS region were 523, 679 and 750 nm, which refer to hematite iron oxide (VISCARRA ROSSEL ET AL., 2006; VISCARRA ROSSEL; BEHRENS, 2010; LUGASSI et al., 2014; FANG et al., 2018). The Fe oxides have a great influence on the color variation in soils and this is shown in the VIS region, making this region one of the most important for the modeling (MORELLOS et al., 2016; TÜMSAVAŞ et al., 2018). Other important peaks of the spectrum for the prediction of sand were in 1910 and 2200 nm, which are characterized as being kaolinite absorption bands. The peak at 2480 nm is related to the presence of Fe-OH.

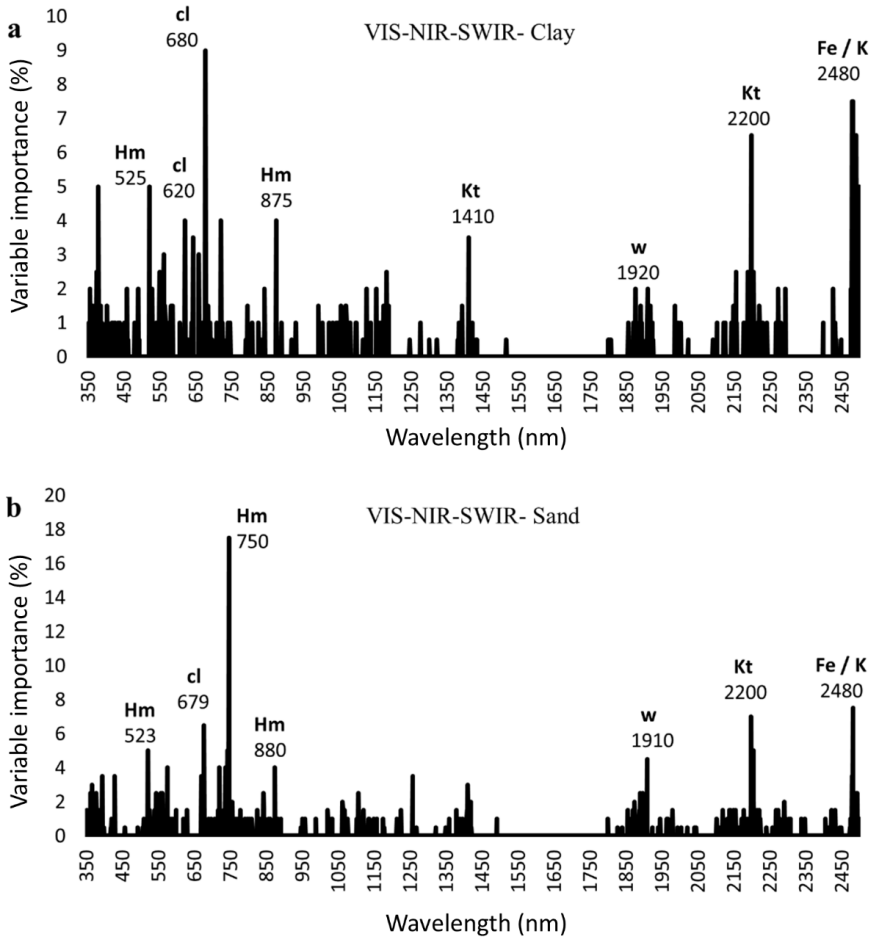

Fig. 6. Variable Importance from VIS-NIR-SWIR models for clay a) and sand content prediction b). Hm: Hematite; cl: Color information; Kt: Kaolinite; w: H-O-H bending in structural/adsorbed H2O; Fe presence of Fe-OH.

In the MIR region, we found the bands that most influenced in the prediction models of clay around 3349 to 3900 cm^{-1}. This range of bands refers to clay minerals, mainly kaolinite between 3600 and 3700 cm^{-1} (NAYAK; SINGH, 2007; SAIKIA; PARTHASARATHY, 2010; DJOMGOUE; NJOPWOUO, 2013; PENG et al., 2014), due to the O-H stretching vibration of the kaolin group. In addition, another important band was in ~3500 cm^{-1} that is associated with O-H stretching of gibbsite (NGUYEN; JANIK; RAUPACH, 1991; TINTI et al., 2015). Also, bands of ~2520, ~1820 and between 1479 and 1408 cm^{-1} are related to carbonates (NGUYEN; JANIK; RAUPACH, 1991). The O-H bending of water was associated with important bands from 1642 to 1569 cm^{-1} (TINTI et al., 2015). The silica spectrum shows importance in the clay model at ~2000 cm^{-1} related to

quartz and O–Si–O stretching of silica between 1135 to 1070 cm^{-1} and 700 cm^{-1} (CALDERÓN; MIKHA; VIGIL, 2011). We also found important absorptions at 611 to 958 cm^{-1}, where there is a peak approximately between 891 to 950 cm^{-1} corresponding to the kaolinite Al-OH curvature vibrations (SAIKIA; PARTHASARATHY, 2010), and 1293 and 1785 cm^{-1}, which is also influenced by kaolinite (PENG et al., 2014).

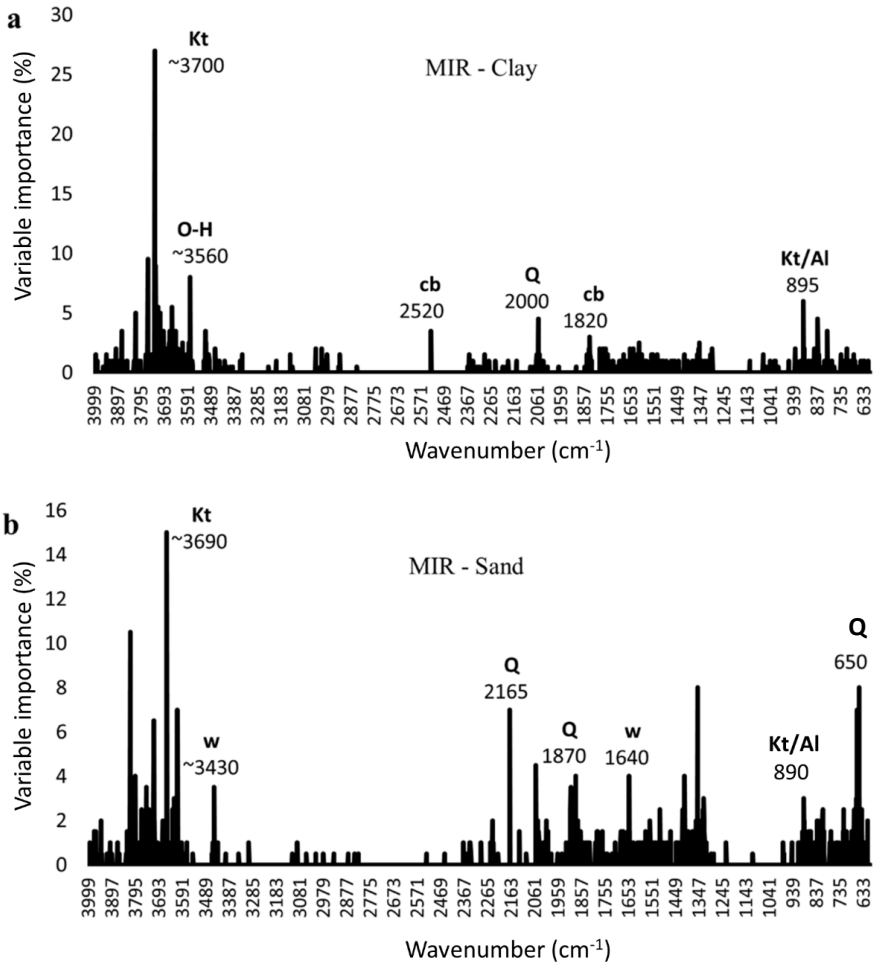

Fig. 7. Variable Importance from MIR models for clay a) and sand content prediction b). Kt: Kaolinite; O-H/Gb: O-H stretching of gibbsite; Cb: Carbonates; Q: Quartz; Kt/Al: kaolinite Al-OH curvature vibrations; w: O–H stretching of H-bonded water.

The main bands to predicting the sand were found at approximately 3690 cm^{-1} and 890 cm^{-1} related to kaolin group (NAYAK; SINGH, 2007; SAIKIA; PARTHASARATHY, 2010; DJOMGOUE; NJOPWOUO, 2013; PENG et al., 2014). Another important region was at ~3430 cm^{-1}, which refer to O–H stretching

of H-bonded water, also between 1642 to 1570 cm^{-1}, which is associated to O-H bending of water (TINTI et al., 2015), and ~ 650 cm^{-1}, that is related to quartz (SILVERO et al., 2020). Other bands were reported at ~2100 to ~1870 cm^{-1} that refers to Si–O vibration of quartz mineral (CAMARGO et al., 2018; LANDRÉ et al., 2018), associated with sand.

Considering the entire VIS-NIR-SWIR region, the VIS was the most important in the clay and sand prediction models. Mainly due to the property of the soil color, dominated by the hematite (Fe oxide), which presents its characteristics in the spectral range. For MIR region, the kaolinite (clay mineral) group had greater influence to distinguish and estimate the clay and sand content.

3.4. Conclusions

The combination of all soil depths led to a more accurate prediction of soil texture fractions when compared to the depth-specific cases. This was due to the variation of the data, which was higher for the total dataset than for the depth-specific data. Therefore, a more accurate prediction can be achieved for data sets with larger standard deviation. The results showed that the variation of the input data is a key factor affecting the final prediction accuracy of soil texture.

Considering the soil texture prediction, by combining all soil depths the three modeling approaches differing in spectral region (VIS-NIR-SWIR, MIR, and combination) enabled to achieve high accuracy for both clay and sand content but very low accuracy for silt content.

Combination of VIS-NIR-SWIR and MIR regions led to similar model performance as when using the MIR region only. The accuracy gained using the combination of VIS-NIR-SWIR and MIR was not relevant. Therefore, the MIR spectroscopy technique can be used to complement the standard soil particle fractions analysis in the routine laboratories processing large number of samples in a short period of time.

The outstanding prediction accuracy achieved using MIR spectral region is related to significant associations between soil mineralogy and soil texture. The

bands with high importance for the soil texture prediction were related specifically to quartz, gibbsite and kaolinite. Thus, the strong mineralogy-to-soil texture relationship helps the quantification of clay and sand content via MIR soil spectroscopy.

4. CAPÍTULO III – IDENTIFICATION OF SOIL MINERALS BY VIS–NIR–SWIR REFLECTANCE SPECTROSCOPY[3]

4.1. Introduction

The typical climate in tropical and subtropical regions allows a wide variety of crops for food production to be successfully grown. However, poor land use and management due to a lack of knowledge of soil properties such as mineralogy in many such regions typically result in low agricultural yields (BAHIA; MARQUES; SIQUEIRA, 2015). Accurately characterizing the mineralogical composition of soils is very important toward understanding soil dynamics in those areas and improving existing land management methods.

Minerals in soils influence the agricultural and environmental characteristics of land (CAMARGO et al., 2015). In fact, the mineralogical composition of soils is known to influence their physical and chemical properties (CLARK et al., 1990; LIMA NETO et al., 2009; OLIVEIRA et al., 2020; REATTO et al., 1998). Thus, soil texture is directly influenced by clay minerals, the content in which has an impact on a number of soil properties including water dynamics. Also, mineral composition (particularly the iron oxides hematite and goethite) dictates to what extent certain nutrients and potentially toxic elements (PTEs) are adsorbed by tropical and subtropical soils (Almeida et al., 2003; Camargo et al., 2012; Sun and Zhang, 2017; Oliveira et al., 2020).

[3] Adapted from article accepted in *Catena Journal* (March/2021).

Soil physical attributes such as texture and structure, and chemical attributes such as phosphorus adsorption and cation-exchange capacity, are governed by the nature and concentration of minerals that are additionally used to classify soils (RAMAROSON et al., 2017; SORIANO-DISLA et al., 2014). The mineralogical composition of soils is usually established by X-ray diffraction (XRD) spectroscopy. This technique, however, is expensive and time-consuming, and uses toxic materials (OMRAN, 2017), so it is impractical for obtaining large data sets or conducting large-scale studies (DUFRÉCHOU; GRANDJEAN; BOURGUIGNON, 2015). These XRD particularities corroborate that mineralogical analysis is not as commonly performed as physical and chemical analysis.

The proximal sensing technique VIS–NIR–SWIR reflectance spectroscopy has become an increasingly used alternative soil scanning technique in replacement of standard soil analysis methods. This technique is fast, non-destructive, inexpensive, environmentally friendly and efficient in determining various soil properties (VISCARRA ROSSEL et al., 2016). Also, it excels conventional techniques in that it provides expanded information on soil attributes from a single spectral measurement (GHOLIZADEH et al., 2020; SACRISTÁN; VISCARRA ROSSEL; RECATALÁ, 2016). In fact, the absorption features, peaks and valleys of VIS–NIR–SWIR reflectance spectra can be used to directly determine soil attributes including mineralogy (TERRA; DEMATTÊ; VISCARRA ROSSEL, 2018). Coblinski et al. (2020) estimated soil texture by reflectance spectroscopy and concluded that the bands providing the best estimates for sand and clay minerals were associated to soil mineralogy. This is a result of certain chemical bonds and molecules absorbing light at specific wavelengths (RAMAROSON et al., 2017). Thus, the VIS region (350–700 nm) provides a spectral signature for chromophores (viz., sets of atoms responsible for color and structure in a molecule) such as hematite and goethite (VISCARRA ROSSEL; BEHRENS, 2010; SORIANO-DISLA et al., 2014). On the other hand, the NIR–SWIR region (700–2500 nm) contains the spectral signatures for clay minerals and soil organic matter (OMRAN, 2017; ZHAO et al., 2018).

Based on the foregoing, some soil attributes and minerals can be identified and quantified from spectral bands at certain wavelengths (SORIANO-DISLA et

al., 2014). However, VIS–NIR–SWIR reflectance spectroscopy has scarcely been used to elucidate soil mineralogy and its relationship to textural class in tropical and subtropical soils.

Because textural classes are associated to particle size fractions, we expected that grouping minerals by class would allow more accurate identification of minerals in soils. This led us to conduct the present work, which was aimed at ascertaining whether VIS–NIR–SWIR reflectance spectra are useful to identify the main mineralogical compositions for characterizing tropical and subtropical soils in different granulometric variation.

4.2. Material and methods

4.2.1. Study area, and soil sampling and analysis

The study area is located in the Brazilian state of Rio Grande do Sul and spans 325 ha (Fig. 8). The parent materials are Igneous rocks (monzogranite and syenogranite) and alluvial deposits (sand and gravel). According to the World Reference Base for Soil Resources (WRB; IUSS Working Group WRB, 2015), land in this area consists of four soil types, namely: Rhodic Acrisols, Xanthic Alisols, Xanthic Acrisols and Dystric Regosols. The Alisols and Acrisols have a textural B horizon underneath A and E; also, they have either low clay activity or high activity with low base saturation. By contrast, the Regosols are poorly developed soils with base saturation < 50% and lacking lithic contact down to 50 cm — if present, B horizon is not thick enough for any subsurface diagnostic horizon. Rhodic Acrisols are present in the smooth, wavy relief in the north and south of the area. Xanthic Acrisols occur in the shallow middle thirds of the slopes, and dystrophic Xanthic Alisols in the lower thirds. Finally, Dystric Regosols constitute the dominant soil type in the steepest locations (viz., the center of the area).

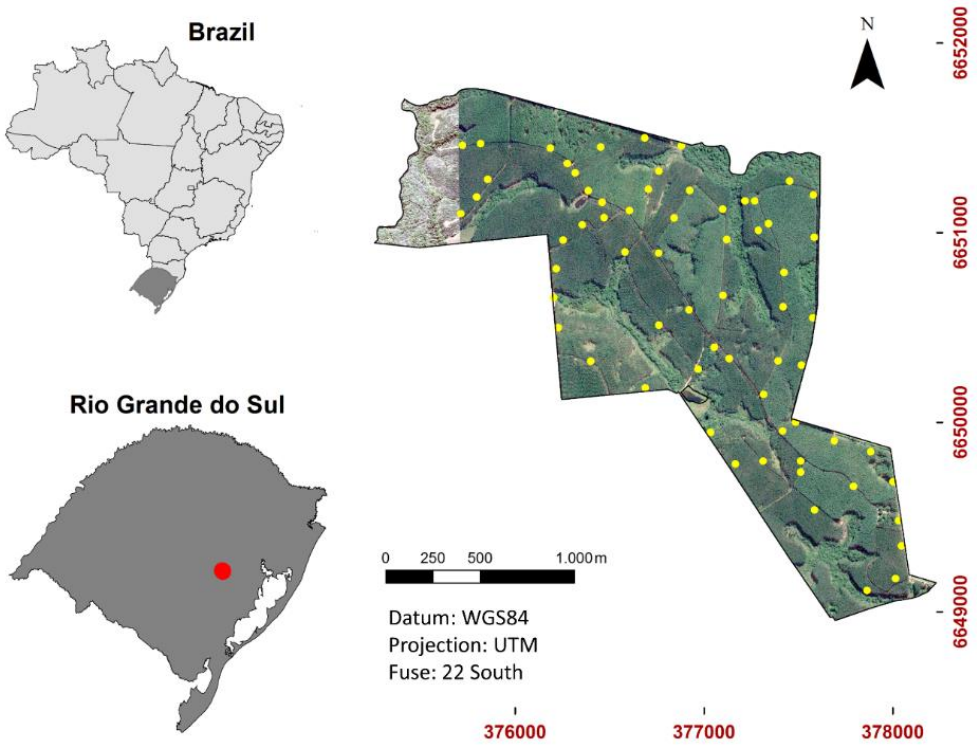

Fig. 8. Study area and location of sampling sites (yellow spots). Image source: Google Earth Pro (2020).

A total of 197 soil samples were collected from three different depths (0.00–0.20, 0.20–0.40 and 0.40–0.60 m) at 66 sampling sites in the Brazilian state of Rio Grande do Sul —the soil at one of sampling point was only 50 cm deep, so only two samples were collected from it. The samples were air-dried, milled and sieved (≤ 2 mm). Particle size fractions (clay, silt and sand) were determined with the pipette method (TEIXEIRA et al., 2017) and the results used to construct a soil texture triangle according to the United States Department of Agriculture (USDA).

4.2.2. Soil spectral measurements

Soil reflectance spectra in the VIS–NIR–SWIR region (350–2500 nm) were obtained by using a FieldSpecPro spectrometer from Analytical Spectral Devices (Boulder, CO, USA) with spectral resolution interpolated to 1 nm. All measurements were made on soil particles smaller than 2 mm. Samples were placed in Petri dishes and homogenized by leveling the surface to reduce the

influence of material roughness. The instrument was calibrated using a white Spectralon standard before each measurement session and then at 20 min intervals during readings. Each sample was measured in triplicate, its Petri dish being rotated 90° between measurements to ensure more accurate representation of the surface area examined. The spectroradiometer automatically used an average of 100 scans for each independent measurement. The overall spectrum for each sample was calculated as the average of its three spectra. Geometry and data acquisition were obtained according to Terra et al. (2015).

4.2.3. Pre-processing of spectral data and evaluation of soil minerals

Figure 9 depicts the procedure used to elucidate the mineralogical composition of the soils from VIS–NIR–SWIR spectral data. The occurrence of soil mineralogy in the study area was verified through previous studies of soils in the same region (AMARAL et al., 2015; CORRÊA DE MEDEIROS et al., 2020; FINK et al., 2014; OLIVEIRA et al., 2020; SILVA et al., 2015). Such studies were conducted at locations with a climate, soil type and parent material similar to those of the study area.

The spectra for pure specimens of the minerals were obtained from the spectral library of the United States Geological Survey (USGS; https://www.usgs.gov/labs/spec-lab), which contains signatures for minerals throughout the world (KOKALY et al., 2017). Identification of mineral signatures was facilitated by applying the continuum removal (CR) algorithm to the spectra for both soil samples and pure minerals. The CR algorithm normalizes reflectance spectra to allow the recognition of diagnostic absorption features of each mineral from a common baseline (CLARK; ROUSH, 1984).

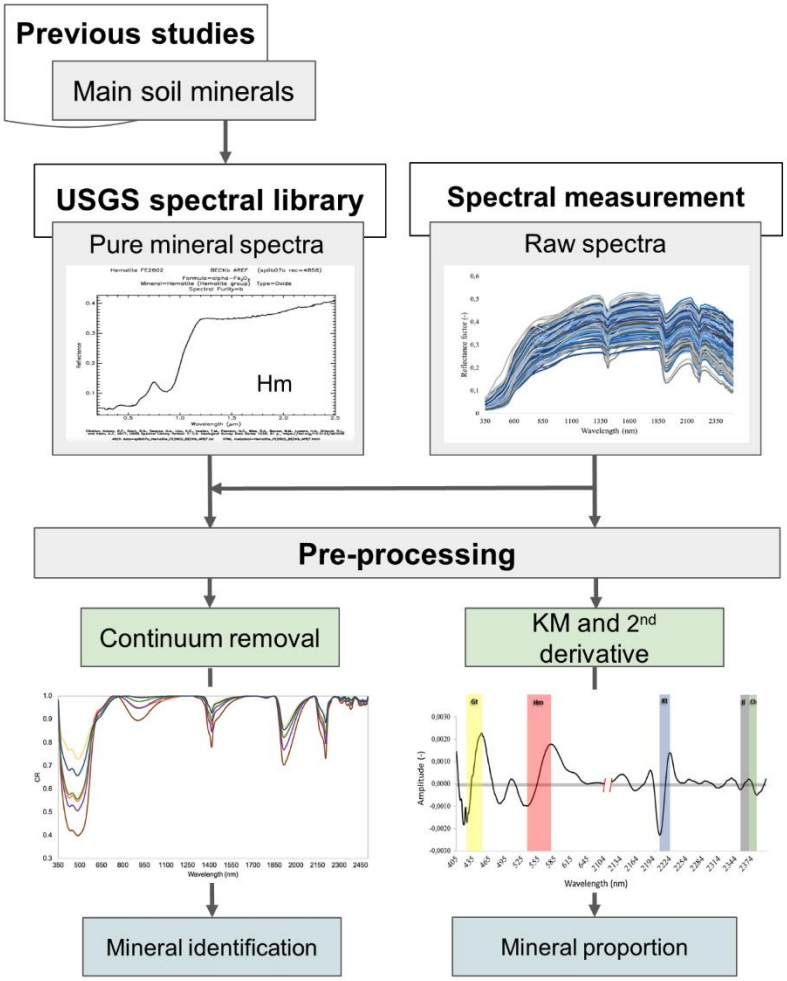

Fig. 9. Procedure for identification of soil minerals and estimation of their proportions.

After minerals were identified by comparing the spectral absorption features of the samples with those of the pure minerals, raw reflectance spectra were applied the Kubelka–Munk (KM), [(1 – *R*) 2/2 *R*] function (where *R* is reflectance). This was followed by calculation of the second-derivative of the function (SCHEINOST et al., 1998). The result of this process was a series of positive and negative bands due to light absorption by effect of electronic transitions (RODRÍGUEZ; FERNÁNDEZ, 2005). Then, curve noise was filtered off by using the Savitzky–Golay weighted combination method to smooth adjacent points with 35 window points (SAVITZKY; GOLAY, 1964) without degradation of the original spectral shape. Mineral types were identified, and proportions estimated, in terms of the amplitude from the maximum intensity to the minimum value for the characteristic band of each mineral in the second-

derivative spectrum (SELLITTO et al., 2009). A ternary diagram of the proportion between oxides and minerals was generated.

A correlogram based on Pearson's correlation was then obtained from the normalized data set in order to better understand the relationship between soil mineralogy and texture. The data were previously scaled, and outliers detected visually in the histogram and removed (MARTENS; NÆS, 1984).

The above-described procedures allowed us to identify subtle, similar absorption features that could not be detected in the pure spectra. The CR algorithm applied was developed in R language (R Development Core Team, Vienna, Austria) as implemented in the Prospectr software package (STEVENS; RAMIREZ-LOPEZ, 2014), and the KM function and its second-derivative were calculated by using Unscrambler® from CAMO Software, Inc. (Montclair, NJ, USA).

4.3. Results and discussion

4.3.1. Soil texture classes and spectral variability

The soil samples were classified by texture according to USDA's criteria. As can be seen in Fig. 10, 77 samples were Sandy Clay Loam, 48 Clay, 42 Sandy Loam, 17 Clay Loam, 7 Sandy Clay, 5 Loamy Sand and 1 Loam. Soil texture thus ranged from very clayey to sandy. Also, clay contents ranged from 5 to 70%, sand contents from 14 to 86% and silt contents from 9 to 47%.

According to Demattê (2002), identifying spectral signatures requires examining albedo (reflectance intensity), absorption features and spectrum shape. The spectral curve features are influenced by soil properties (physical, chemical, biological and mineralogical), all of which affect reflectance intensity, absorption, and spectrum depth and bandwidth. In clayey soils, absorption features are made more prominent by the presence of increased amounts of pigmenting minerals in the clay fraction. This is especially so with iron oxides such as hematite and goethite in the wavelength region 400–700 nm, and with clay minerals (kaolinite, mainly) in the 2200 nm region. On the other hand, high reflectance intensities prevail in soils containing more quartz than other minerals

(COBLINSKI et al., 2020; DEMATTÊ et al., 2014; XU et al., 2017; YU; HUNT, 2018).

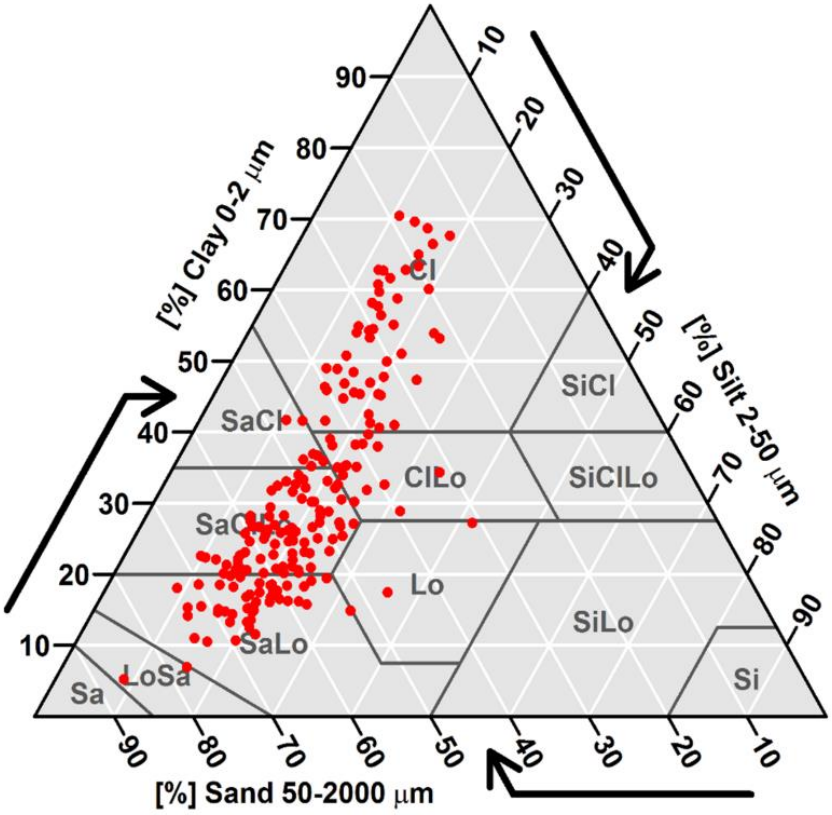

Fig. 10. Classification of the soil samples by texture.

Figure 11 shows the mean continuum-removed spectra by texture classes. As can be seen, the Clay, Clay Loam and Sandy Clay textural classes, all of which contained more clay than the others, exhibited greater, more apparent absorption by effect of the presence of large amounts of iron oxides and clay minerals. This is clearly reflected in the absorption features of the bands for goethite (Gt; 420 nm, 485 nm and 920 nm), which exhibited increased absorption in these textural classes. Although the Clay, Clay Loam and Sandy Clay textural classes exhibited more marked absorption features in the band at ca. 920 nm for Gt; the CR spectrum can be influenced by other minerals such as hematite (Hm), which has an absorption feature in the 860–880 nm region (CLOUTIS et al., 2016; HAUFF, 2007; PRADO et al., 2016; VISCARRA ROSSEL et al., 2010).

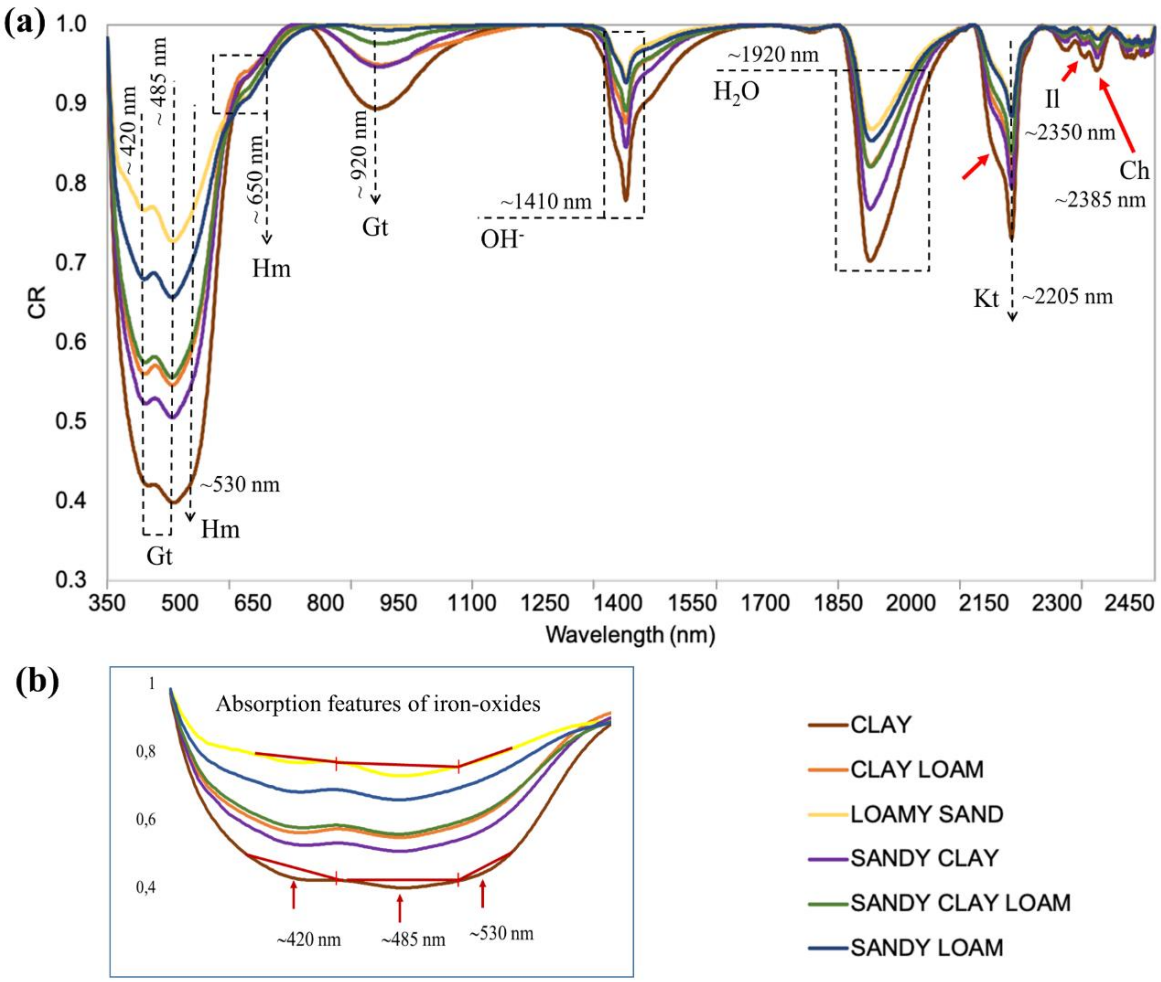

Fig. 11. a) Mean continuum removed spectra (CR) by texture classes of 197 soil samples. b) Absorption features of iron oxides in the visible region (VIS) —the Loam texture class is not shown because it comprised only one sample.

The CR procedure failed to clearly expose the absorption feature of the 530 nm band for Hm (Figs 11a and 11b). Zooming on the visible region for Gt and Hm (Fig. 11b) revealed that the band at ca. 530 nm, which is typically used to quantify hematite, was less marked than those for Gt —and hence that the soils contained more Gt than Hm. In addition, the band at 530 nm for Hm was broad, whereas those at 420 and 480 nm for Gt were narrow, which hindered identification of the Hm signature in the CR spectra (FANG et al., 2018).

Soils in the three textural classes with the highest sand contents (viz., Loamy Sand, Sandy Loam and Sandy Clay Loam) exhibited an especially prominent absorption feature in the 650 nm band for Hm, whereas those in the other three classes showed no absorption features (Fig. 11a). Iron oxides were

present mainly in the clay fraction, but were also found as residual minerals resisting weathering of the parent materials in the sandy fraction (COSTA; BIGHAM, 2009) or as coatings of quartz minerals.

The highest Kt absorptions (2205 nm) also occurs in the Clay, Clay Loam and Sandy Clay textural classes. Also, the minerals illite (Il) and chlorite (Ch) exhibited moderate but greater absorption in these three classes than in those with the highest sand contents (Loamy Sand, Sandy Loam and Sandy Clay Loam; Fig. 11). The OH vibrational groups (1410 and 1920 nm), have more intense absorption features in the three textural classes with higher clay contents and apparently more goethitic, because they refer to OH^- and H_2O stretching vibration of clay minerals, such as the kaolinite group (BEN-DOR; BANIN, 1995; COBLINSKI et al., 2020). In addition, the spectrum for Gt included a weak absorption band at around 1700 nm corresponding to the first overtone of an O–H stretching vibration present in the crystal structure of the mineral (STENBERG et al., 2010).

4.3.2. Mineralogical composition of the soils

As can be seen in Fig. 12, the soils contained five different minerals, namely: the iron oxides hematite (Ht) and goethite (Gt), and the clay minerals kaolinite (Kt), chlorite (Ch) and illite (Il). Hematite and goethite, which are the most abundant iron oxides in weathered soils in tropical and subtropical regions, can be easily identified from spectral curves as a result of the sharp separation that the second-derivative performs (SCHEINOST et al., 1998; SELLITTO et al., 2009). The spectral signatures of iron oxides are identified in the visible region (350–700 nm), together with the chromophores signature (SORIANO-DISLA et al., 2014; VISCARRA ROSSEL; BEHRENS, 2010). Fig. 12 indicates that for goethite, the amplitude was identified with a minimum around 420 nm and a maximum at 460 nm, matching the spectral signature from other studies (BAHIA; MARQUES; SIQUEIRA, 2015; FANG et al., 2018; SELLITTO et al., 2009).

According to Scheinost et al. (1998), the identification of hematite in pure spectra (raw spectra) is apparent around 520 nm to 565 nm. In the current study, with the transformation of the second-derivative, the amplitudes for hematite were identified with the minimum at ~535 nm and maximum at ~580 nm (Fig. 12). This

same range of absorption bands referring to hematite in the curves of the second-derivative was also found by other authors (BAHIA; MARQUES; SIQUEIRA, 2015; FANG et al., 2018; SELLITTO et al., 2009).

The 1:1 clay mineral kaolinite was also identified (Fig. 12). Kaolinite (Kt) occurs in a wide variety of soils and is the most common mineral in soils developed under humid tropical conditions in Brazil (e.g., Acrisols and Oxisols; OLIVEIRA et al., 2020). This clay mineral forms mainly by dissolution of primary minerals, and back-precipitation of Si and Al. For example, feldspars often become kaolinite in soils formed from igneous rocks (MELO; WYPYCH, 2009; SCHULZE; LAFAYETTE, 2002). The reflectance spectrum for Kt exhibits a strong absorption feature at 2205 nm and a weaker one at 2165 nm (CLARK et al., 1990; VISCARRA ROSSEL et al., 2010). The absorption features for Kt in the second-derivative spectrum include a minimum at ca. 2205 nm and a maximum at ca. 2225 nm (MADEIRA et al., 1995; POPPIEL et al., 2019); as can be seen in Fig. 12 (2204 nm and 2226 nm, respectively).

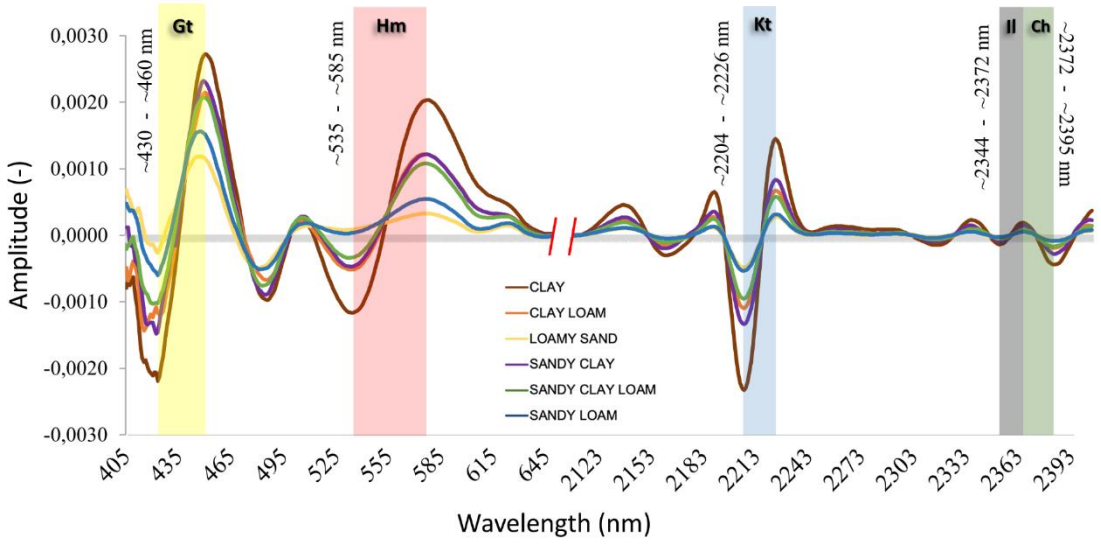

Fig. 12. Spectral signature of soil minerals through second-derivative of KM function in the VIS–NIR–SWIR region (350–2500 nm). Gt goethite; Hm hematite; Kt Kaolinite; Il Illite; Ch Chlorite. The 350–404 and 657–2104 nm regions have been excluded because they contained no significant spectral signatures.

Chlorite and illite were other identified minerals (Fig. 12). Illite is a 2:1 clay mineral absorbing light at ca. 1400, 1900 and 2350 nm (CLARK et al., 1990; POPPIEL et al., 2019; STENBERG, 2010), and exhibiting a minimum at 2344–

2358 nm and a maximum at 2360–2372 nm in the second-derivative spectrum (Fig. 12). Chlorite is another 2:1 clay mineral but contains excess negative charge and specific octahedral cations such as Fe, Al and Mg. The raw spectrum for Ch exhibits an absorption feature at ca. 1400 nm and three others at ca. 2300 nm (CLARK et al., 1990; FANG et al., 2018; ZHAO et al., 2017), with the spectral signature at 2385 nm. The amplitude of the second-derivative spectrum for Ch was defined by a minimum at 2372–2395 nm and a maximum at 2355–2370 nm (Fig. 12). According to Zhao et al. (2017), the presence of Ch and Il is suggestive of mild weathering under cold and temperate conditions. However, Ch is a primary mineral inherited from igneous, metamorphic or even sedimentary rocks, and is usually present in small amounts (SCHULZE; LAFAYETTE, 2002). Il is highly resistant to weathering, so it is usually a remnant of the parent material (JACKSON; SHERMAN, 1953; XU et al., 2017).

4.3.3. Relationship of soil texture class to minerals and proportions

The relationship between soil texture classes and minerals was examined by constructing the correlogram of Fig. 13. As can be seen, sand and clay were highly correlated in a negative and positive manner, respectively, with the minerals. The highest correlation among clay and minerals was observed with kaolinite (r = 0.84) and illite the lowest (r = 0.69). On the other hand, sand was highly correlated in a negative manner with all minerals ($r \geq -0.62$), while silt was poorly correlated with all minerals possibly due to its lower proportion in most samples as shown by Coblinski et al. (2020).

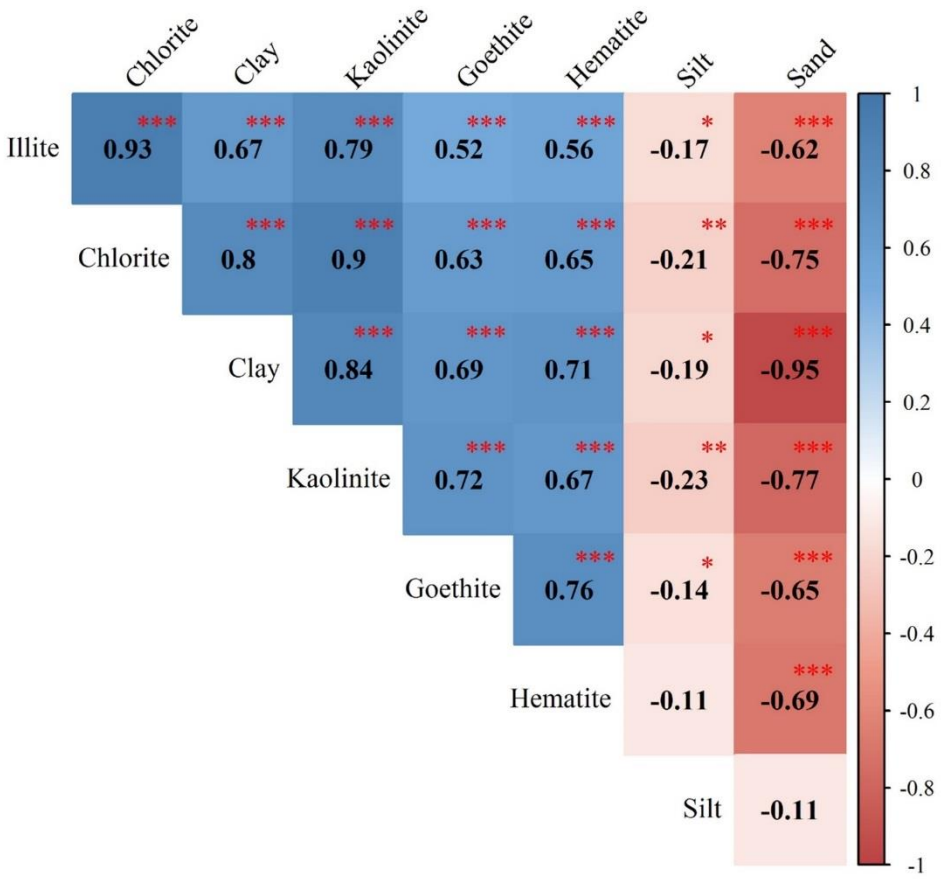

Fig. 13. Pearson correlogram between minerals as identified by reflectance spectroscopy and soil particles as determined with standard methods (*** $p < 0.001$, ** $p < 0.01$, * $p < 0.05$).

As can be seen from Fig. 14a, the higher was the proportion of clay in the soil, the greater was band amplitude for clay minerals and iron oxides in the second-derivative spectrum. Figure 14b shows the spectral signatures for each mineral identified; also, it compares the textural classes Clay and Loamy Sand, which are more clayey and sandy, respectively. As can be seen, these two classes differed markedly in spectral amplitude. The amplitudes of the spectral signatures, which reflect the proportions of the minerals, were greatest for the textural class with the highest clay content (viz., the Clay class). This was a result of the minerals being components of the clay structure (SANTOS; ALMEIDA; SEQUINATTO, 2017). The contents in iron oxides (Hm and Gt) and kaolinite (Kt) where higher than those in 2:1 clay minerals (Il and Ch) irrespective of textural class.

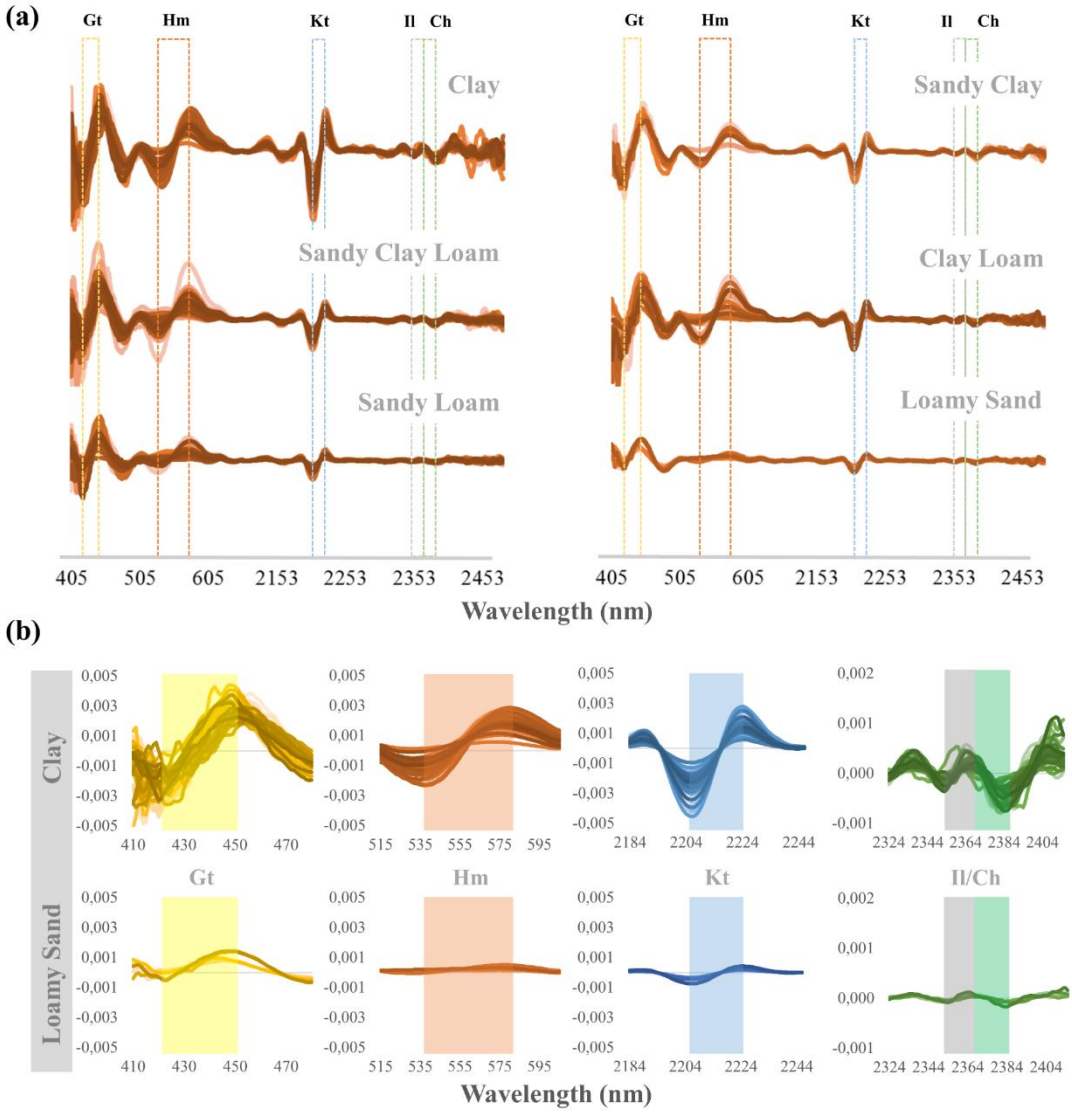

Fig. 14. a) Second-derivative of the KM function for the samples as classified according to texture. The 657–2104 nm region was excluded because it contained no significant spectral signatures. b) Spectral signature and amplitude for each mineral in the Clay and Loamy Sand texture classes.

Figure 15 shows the ternary diagrams used to represent the proportions of iron oxides and Kt. The high contents in Hm and Gt are consistent with those of Bigham et al. (2002), according to whom these two minerals are the main iron oxides in tropical soils. Our soils contained Kt mainly. The high availability of Fe oxides, and 1:1 clay minerals, in the clay fraction suggests that soils in the study area are well-weathered. Consequently, they probably contain low levels of nutrients as a result of Kt being the most abundant 1:1 clay mineral in them and

its containing no large cations (K, Ca, Mg) or nutrient elements in its structure (KÄMPF; CURI, 2003).

As can be seen from Figs 15b–15f, Gt was generally found a higher proportion than was Hm in all textural classes except Clay —which contained iron oxides and Kt in similar proportions (Fig. 15a). Goethite can be found in almost any type of environment but mostly during weathering of soil—Gt is the most stable iron oxide at ambient temperature and pressure (BIGHAM; FITZPATRICK; SCHULZE, 2002). Although this mineral prevailed in our subtropical soils, its color may have been masked by the reddish hues of Hm in some cases (SCHWERTMANN, 1993).

According to Totsche et al. (2018), iron oxides and clay minerals are directly associated to soil aggregation; also, they are the most important mineral phases in the formation of microaggregates. Because of the high cementing power of oxides, their removal causes soil particles to break down (PINHEIRO-DICK; SCHWERTMANN, 1996). As a result, soils with high iron oxide contents possess a very stable structure (BORGGAARD, 1983).

As can be seen from Figs 14 and 15, the soils with increased clay contents contained iron oxides and clay minerals in higher proportions. Such soils contained more microaggregates, which increase stability, water retention and volume porosity, thereby facilitating aeration of plants.

Minerals reflect the degree of weathering of soils and govern their ability to retain various elements such as phosphorus, thereby influencing soil fertility, health and quality (CAMARGO et al., 2012; HONG et al., 2019). Therefore, using an efficient technique such as VIS–NIR–SWIR spectroscopy to determine the mineralogical composition of soils as a supplement to physicochemical analyses can help improve agricultural practices and assist decision-making in agricultural support policies.

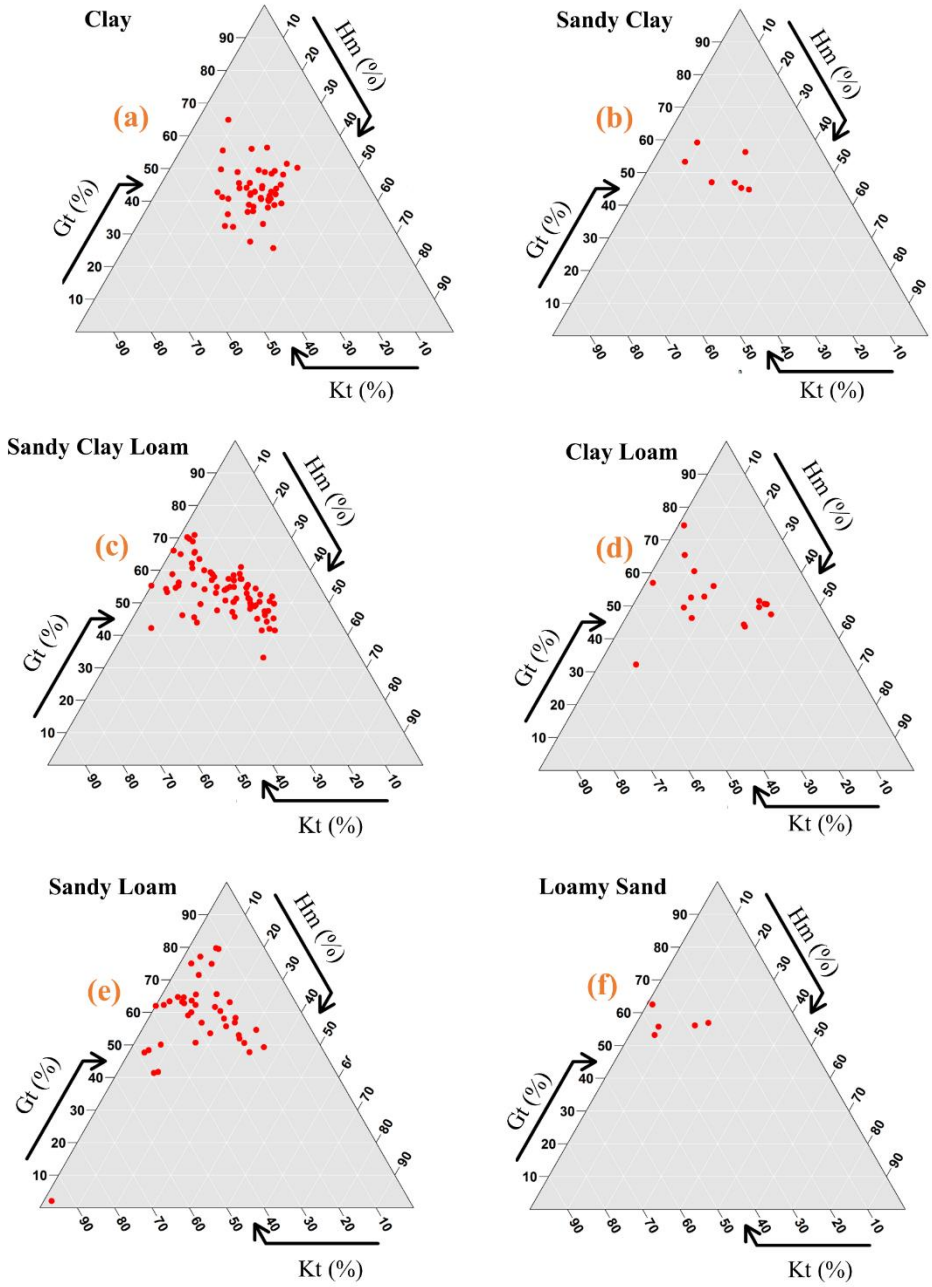

Fig. 15. Ternary diagrams of mineral proportions in the different soil texture classes. (The Loam class is not shown because it comprised only one sample).

4.4. Conclusions

In this work, we determined the relative abundance of the main minerals in subtropical soils from Southern Brazil by VIS–NIR–SWIR reflectance

spectroscopy. The iron oxide goethite was detected in the region 430–460 nm and the hematite in the region 535–585 nm. And the clay minerals kaolinite, illite and chlorite in the regions 2204–2226, 2344–2372 and 2372–2270 nm were found, respectively.

The textural classes with higher clay contents had increased proportions of iron oxides and clay minerals such as kaolinite. Moreover, the class with the highest sand content (Loamy Sand) showed the least marked spectral absorption features.

Based on the results, VIS–NIR–SWIR reflectance spectroscopy successfully identified the mineral composition of the soils determining accurately, operational expeditiousness and eco-friendly. On the other hand, we showed that the separation of samples by textural class facilitated the identification of minerals. Despite this, the method obtained a more complete analysis of soil characterization and rapid interpretation as to soil texture and mineralogy, which can improve support to agricultural decision making and public policies. Therefore, it can provide an effective supplement for XRD analyses of large sets of soil samples.

5. CAPÍTULO IV - CONSIDERAÇÕES FINAIS

Nesta tese, buscou-se apresentar a técnica da espectroscopia de reflectância para análise de propriedades do solo de importância agrícola e ambiental. O estudo 1 (capítulo II) mostrou que a espectroscopia de refletância nas regiões VIS-NIR-SWIR e MIR é capaz de realizar a predição dos teores das frações areia e argila, devido à grande correlação dessas frações com as bandas espectrais relacionadas à mineralogia do solo. Porém, a região espectral MIR obteve os melhores resultados tanto para treinamento do modelo quanto para a validação da predição da areia e argila, e isso se deveu às maiores quantidades de feições de absorção relacionadas à mineralogia, como, por exemplo o quartzo, que tem características identificáveis nessa região, diferentemente da região VIS-NIR-SWIR, onde o quartzo influenciará apenas na intensidade de refletância na curva espectral como um todo.

Além disso, este estudo foi capaz de demonstrar que resultados com boa acurácia podem ser alcançados sem a necessidade de pré-processamento espectral, apenas utilizando o espectro puro. O estudo 1 também destacou que a subdivisão do conjunto de dados por profundidade interferiu na acurácia da calibração e da validação dos modelos de predição, ou seja, a utilização de todas as amostras de solo, como um só conjunto de dados, melhorou a acurácia de predição do teor de textura do solo, devido à maior heterogeneidade das amostras, ajudando, assim, com a maior variabilidade dos teores, na calibração dos modelos de predição.

Já o estudo 2 (capítulo III) expôs a eficiência da espectroscopia de refletância nas regiões VIS-NIR-SWIR em identificar os principais minerais e suas proporções. Essa metodologia foi capaz de identificar os principais óxidos de ferro (hematita e goetita), argilominerais 1:1 (caulinita) e até mesmo argilomineral 2:1 (ilita e clorita), que são encontrados em baixas concentrações nesses solos. E, ainda, com a transformação da curva espectral na segunda derivada, nós obtivemos as amplitudes relacionadas a mineralogia e, através disso, obtivemos a proporção de cada mineral na mesma amostra. Ademais, esse estudo destacou a grande correlação que os valores de amplitude relacionada aos minerais identificados têm com as frações granulométricas do solo, sendo que, com essa análise, pode-se ter uma interpretação prévia da condição do solo analisado, auxiliando assim para tomadas de decisão agrícola.

Esta tese contribuiu para o avanço de estudos da espectroscopia de refletância aplicada à ciência do solo, mostrando que essa técnica está apta para realizar análises da textura do solo, diminuindo o uso de reagentes químicos e reduzindo o tempo de análise. Devido à alta acurácia alcançada, pode-se afirmar que o sensor na região espectral MIR pode complementar a análise padrão de textura do solo. A tese ainda contribuiu para a análise interpretativa do solo de maneira rápida, isto é, para a identificação rápida e de forma simples da composição mineralógica do solo e das suas proporções através das regiões espectrais VIS-NIR-SWIR. Isso mostra que a espectroscopia também pode ser eficaz com o levantamento de atributos do solo que não são comumente realizados por ser muito custoso e demorado usar muitos reagentes, como no caso da mineralogia. Com a metodologia aqui apresentada, foi descartado o uso de reagentes e foi realizada uma análise relativamente rápida. A partir disso, pode-se ter uma primeira interpretação do solo de uma área estudada.

Trabalhos futuros devem ser realizados para consolidar a utilização da espectroscopia de refletância em estudos aplicados, como proceder à identificação da mineralogia diretamente em campo com sensores portáteis, tendo uma resposta rápida e podendo, dessa forma, realizar uma interpretação da condição do solo em tempo real, através das assinaturas espectrais dos minerais. Além disso, obter a correlação entre essas assinaturas espectrais com os atributos químicos do solo, como o fósforo e o potássio, que são elementos

muito importantes na agricultura e que sofrem grande influência da mineralogia, obtendo assim mais uma análise para interpretação do solo através da curva espectral.

6. Referências Bibliográficas

ALMEIDA, J. A.; TORRENT, J.; BARRÓN, V. Cor de solo, formas do fósforo e adsorção de fosfatos em latossolos desenvolvidos de basalto do extremo-sul do Brasil. **Revista Brasileira de Ciência do Solo**, Viçosa, MG, v. 27, n. 2, p. 985–1002, 2003.

AMARAL, Francisco Hélcio Canuto *et al*. Produtividade *de Eucalyptus grandis* e sua relação com a cinética de liberação de macronutrientes. **Scientia Forestalis**, Piracicaba, v. 43, n. 108, p. 979–991, 2015.

BAHIA, Angélica Santos Rabelo; MARQUES, José; SIQUEIRA, Diego Silva. Procedures using diffuse reflectance spectroscopy for estimating hematite and goethite in Oxisols of São Paulo, Brazil. **Geoderma Regional**, Amsterdam, v. 5, p. 150–156, 2015.

BEN-DOR, E.; BANIN, A. Near-infrared analysis as a rapid method to simultaneously evaluate several soil properties. **Soil Science Society of America Journal**, Madison, v. 59, n. 2, p. 364–372, 1995.

BENEDET, Lucas *et al.* Soil texture prediction using portable x-ray fluorescence spectrometry and visible near-infrared diffuse reflectance spectroscopy. **Geoderma**, Amsterdam, v. 376, [art.] 114553, 2020.

BIGHAM, J. M.; FITZPATRICK, R. W.; SCHULZE, D. G. Iron oxides. *In*: DIXON, J. B.; SCHULZE, D. G. **Soil mineralogy with environmental applications**. Madison: Soil Science Society of America, 2002. p. 323–366.

BLANCO-CANQUI, H.; LAL, R. **Principles of soil conservation and management**. Dordrecht: Springer, 2010. 696 p.

BORGGAARD, O. K. Iron oxides in relation to aggregation of soil particles. **Acta Agriculturae Scandinavica**, Stockholm, v. 33, n. 3, p. 257–260, 1983.

BOWERS, S. A.; HANKS, R. J. Reflection of radiant energy from soils. **Soil Science**, New Brunswick, v. 100, n. 2, p. 130–138, 1965.

BROOKS, F. A. Atmospheric radiation and its reflection from the ground. **Journal of Meteorology**, Lancaster, v. 9, p. 41–52, 1952.

CALDERÓN, Francisco J. *et al*. Diffuse-reflectance mid-infrared spectral properties of soils under alternative crop rotations in a semi-arid climate. **Communications in Soil Science and Plant Analysis**, Basingstoke, v. 42, n. 17, p. 37–41, 2011.

CAMARGO, Livia Arantes *et al.* Spatial correlation between the composition of the clay fraction and contents of available phosphorus of an Oxisol at hillslope scale. **Catena**, Cremlingen, v. 100, p. 100–106, 2012.

CAMARGO, Livia Arantes *et al.* Mapping of clay, iron oxide and adsorbed phosphate in Oxisols using diffuse reflectance spectroscopy. **Geoderma**, Amsterdam, v. 251/252, p. 124–132, 2015.

CAMARGO, Livia Arantes *et al.* Predicting potentially toxic elements in tropical soils from iron oxides, magnetic susceptibility and diffuse reflectance spectra. **Catena**, Cremlingen, v. 165, p. 503–515, 2018.

CAMBOU, Aurélie *et al.* Prediction of soil organic carbon stock using visible and near infrared reflectance spectroscopy (VNIRS) in the field. **Geoderma**, Amsterdam, v. 261, p. 151–159, 2016.

CHANG, Cheng-Wen *et al.* Near-infrared reflectance spectroscopy–principal components regression analyses of soil properties. **Soil Science Society of America Journal**, Madison, v. 65, n. 2, p. 480-490, 2001.

CHANG, Cheng Wen; LAIRD, David A. Near-infrared reflectance spectroscopic analysis of soil C and N. **Soil Science**, New Brunswick, v. 167, n. 2, p. 110–116, 2002.

CLARK, Roger N. *et al.* High spectral resolution reflectance spectroscopy of minerals. **Journal of Geophysical Research**, Hoboken, v. 95, n. B8, p. 12653-12680, 1990.

CLARK, Roger N.; ROUSH, T. L. Reflectance spectroscopy: quantitative analysis techniques for remote sensing applications. **Journal of Geophysical Research**, Hoboken, v. 89, n. B7, p. 6329–6340, 1984.

CLOUTIS, Edward *et al.* Identification of historic artists' pigments using spectral reflectance and X-ray diffraction properties I. Iron oxide and oxy-hydroxide-rich pigments. **Journal of Near Infrared Spectroscopy**, London, v. 24, n. 1, p. 27–45, 2016.

COBLINSKI, J. A. *et al.* Prediction of soil texture classes through different wavelength regions of reflectance spectroscopy at various soil depths. **Catena**, Cremlingen, v. 189, [art.] 104485, 2020.

COSTA, A. C.; BIGHAM, Jerry M. VIII – Óxidos de ferro. *In*: MELO, V. F.; ALLEONI, L. R. F. (ed.). **Química e mineralogia do solo:** conceitos básicos e aplicações. Viçosa, MG: SBCS, 2009. p. 1381.

CURCIO, D. *et al.* Prediction of soil texture distributions using VNIR-SWIR reflectance spectroscopy. **Procedia Environmental Sciences**, Amsterdam, v. 19, p. 494–503, 2013.

D'ACQUI, L. P.; PUCCI, A.; JANIK, L. J. Soil properties prediction of western Mediterranean islands with similar climatic environments by means of mid-infrared diffuse reflectance spectroscopy. **European Journal of Soil Science**, Oxford, v. 61, n. 6, p. 865–876, 2010.

DEMATTÊ, J. A. M. *et al.* Determining soil water status and other soil

characteristics by spectral proximal sensing. **Geoderma**, Amsterdam, v. 135, p. 179–195, 2006.

DEMATTÊ, J. A. M.; TERRA, Fabrício S. Spectral pedology: a new perspective on evaluation of soils along pedogenetic alterations. **Geoderma**, Amsterdam, v. 217/218, p. 190–200, 2014.

DEMATTÊ, J. A. M. Characterization and discrimination of soils by their reflected electromagnetic energy. **Pesquisa Agropecuária Brasileira**, Brasília, DF, v. 37, n. 10, p. 1445–1458, 2002.

DEMATTÊ, J. A. M. *et al.* Morphological Interpretation of Reflectance Spectrum (MIRS) using libraries looking towards soil classification. **Scientia Agricola**, Piracicaba, v. 71, n. 6, p. 509–520, 2014.

DICK, D. P.; SCHWERTMANN, U. Microaggregates from oxisols and inceptisols: dispersion through selective dissolutions and physicochemical treatments. **Geoderma**, Amsterdam, v. 74, n. 1/2, p. 49–63, 1996.

DJOMGOUE, Paul; NJOPWOUO, Daniel. FT-IR spectroscopy applied for surface clays. **Journal of Surface Engineered Materials and Advanced Technology**, Irvine, v. 3, n. 4, p. 275–282, 2013.

DUDA, Bogdan M. *et al.* Soil characterization across catenas via advanced proximal sensors. **Geoderma**, Amsterdam, v. 298, p. 78–91, 2017.

DUFRÉCHOU, G.; GRANDJEAN, G.; BOURGUIGNON, A. Geometrical analysis of laboratory soil spectra in the short-wave infrared domain: clay composition and estimation of the swelling potential. **Geoderma**, Amsterdam, v. 243/244, p. 92–107, 2015.

EMBRAPA - EMPRESA BRASILEIRA DE PESQUISA AGROPECUARIA. **Sistema brasileiro de classificação de solos**. Rio de Janeiro: Embrapa Solos. Brasília, DF: Embrapa, 2013. 353 p.

FANG, Qian *et al.* Visible and near-infrared reflectance spectroscopy for investigating soil mineralogy : a review. **Journal of Spectroscopy**, New York, v. 2018, [art.] ID 3168974, 2018.

FAO - FOOD AND AGRICULTURE ORGANIZATION OF THE UNITED NATIONS. **World reference base for soil resources 2014:** International soil classification system for naming soils and creating legends for soil maps: update 2015. Rome: FAO, 2015. (World Soil Resources Reports, 106).

FINK, Jessé Rodrigo *et al*. Chemical and mineralogical changes in a Brazilian Rhodic Paleudult under different land use and managements. **Revista Brasileira de Ciência do Solo**, Viçosa, MG, v. 38, n. 4, p. 1304–1314, 2014.

GHIDIN, André Ademir *et al*. Oxisol toposequences developed from basaltic rocks in Paraná State, Brazil. II - Relationship between clay fraction mineralogy and physical soil properties. **Revista Brasileira de Ciência do Solo**, Viçosa,

MG, v. 30, n. 2, p. 307–319, 2006.

GHOLIZADEH, Asa *et al*. Modelling potentially toxic elements in forest soils with vis–NIR spectra and learning algorithms. **Environmental Pollution**, v. 267, [art.] 115574, 2020.

GOMEZ, Cécile; LAGACHERIE, Philippe; COULOUMA, Guillaume. Continuum removal versus PLSR method for clay and calcium carbonate content estimation from laboratory and airborne hyperspectral measurements. **Geoderma**, Amsterdam, v. 148, n. 2, p. 141–148, 2008.

HAUFF, Phoebe. **An overview of VIS-NIR-SWIR field spectroscopy as applied to precious metals**. Arvada: Spectral International, 2007. 71 p.

HENAKA ARACHCHI, M. P. N. K.; FIELD, D. J.; MCBRATNEY, A. B. Quantification of soil carbon from bulk soil samples to predict the aggregate-carbon fractions within using near- and mid-infrared spectroscopic techniques. **Geoderma**, Amsterdam, v. 267, p. 207–214, 2016.

HILLEL, Daniel. **Environmental soil physics:** fundamentals, applications, and environmental considerations. Amsterdam: Academic Press, 1998.

HONG, Yongsheng *et al.* Cadmium concentration estimation in peri-urban agricultural soils: using reflectance spectroscopy, soil auxiliary information, or a combination of both? **Geoderma**, Amsterdam, v. 354, [art.] 113875, [p. 1–14], 2019.

HUNT, Graham R.; SALISBURY, John W. Visible and near-infrared spectra of minerals and rocks: I silicate minerals. **Modern Geology**, London, v. 1, p. 283-300, 1970.

JACKSON, M. L.; SHERMAN, G. D. Chemical weathering of minerals in soil. **Advances in Agronomy**, San Diego, v. 5, p. 221–318, 1953.

JANIK, L. J.; FORRESTER, S. T.; RAWSON, A. The prediction of soil chemical and physical properties from mid-infrared spectroscopy and combined partial least-squares regression and neural networks (PLS-NN) analysis. **Chemometrics and Intelligent Laboratory Systems**, Amsterdam, v. 97, n. 2, p. 179–188, 2009.

JANIK, L. J.; SKJEMSTAD, J. O. Characterization and analysis of soils using mid-infrared partial least-squares. II. Correlations with some laboratory data. **Australian Journal of Soil Research**, Melbourne, v. 33, n. 4, p. 637–650, 1995.

JANIK, L. J.; SKJEMSTAD, J. O.; MERRY, R. H. Can mid infrared diffuse reflectance analysis replace soil extractions? **Australian Journal of Experimental Agriculture**, East Melbourne, v. 38, n. 7, p. 681-698, 1998.

JIANG, Qinghu *et al.* Estimation of soil organic carbon and total nitrogen in different soil layers using VNIR spectroscopy: effects of spiking on model

applicability. **Geoderma**, Amsterdam, v. 293, p. 54–63, 2017.

KÄMPF, N.; CURI, N. Argilominerais em solos brasileiros. **Tópicos em Ciência do Solo**, Viçosa, MG, v. 3, p. 1-54, 2003.

KÄMPF, N.; CURI, Nilton; MARQUES, João José. Intemperismo e ocorrência de mineiras no ambiente do solo. *In*: MELO, V. F.; ALLEONI, L. R. F. (ed.). **Química e mineralogia de solos**. Viçosa, MG: SBCS, 2009. cap. 5, p. 333–379.

KHOSRAVI, Vahid; DOULATI ARDEJANI, Faramarz; YOUSEFI, Saeed. Spectroscopic-based assessment of the content and geochemical behaviour of arsenic in a highly heterogeneous sulphide-rich mine waste dump. **Environmental Earth Sciences**, Heidelberg, v. 76, [art.] 459, [p. 1–16], 2017.

KLEIN, Vilson *et al.* Textura do solo e a estimativa do teor de água no ponto de murcha permanente com psicrômetro. **Ciência Rural**, Santa Maria, v. 40, n. 7, p. 1550-1556, 2010.

KNOX, N. M. *et al.* Modelling soil carbon fractions with visible near-infrared (VNIR) and mid-infrared (MIR) spectroscopy. **Geoderma**, Amsterdam, v. 239/240, p. 229–239, 2015.

KOKALY, Raymond F. *et al.* **USGS spectral library version 7**. Denver: USGS Crustal Geophysics and Geochemistry Science Center, 2017. 61 p. (U.S. Geological Survey Data Series, 1035). Disponível em: https://pubs.er.usgs.gov/publication/ds1035. Acesso em: 5 jan. 2020.

KRAEMER, F. B. *et al*. Soil texture as a regulating factor of *Escherichia coli* adsorption in a rolling pampa basin (Argentina). Revista Argentina de Microbiología, Buenos Aires, v. 43, n. 2, p. 87–93, 2011.

KUHN, Max; QUINLAN, Ross. **Cubist:** rule- and instance-based regression modeling. [Boston: R Foundation for Statistical Computing], 2018. 13 p. Disponível em: https://cran.r-project.org/web/packages/Cubist/index.html. Acesso em: 2 fev. 2019.

LAL, Rattan. **Principles of soil physics**. New York: CRC Press, 2004.

LANDRÉ, A. *et al.* Prediction of total silicon concentrations in french soils using pedotransfer functions from mid-infrared spectrum and pedological attributes. **Geoderma**, Amsterdam, v. 331, p. 70–80, 2018.

LE GUILLOU, F. *et al.* How does grinding affect the mid-infrared spectra of soil and their multivariate calibrations to texture and organic carbon? **Soil Research**, Collingwood, v. 53, n. 8, p. 913–921, 2015.

LIMA NETO, José Almeida *et al.* Caracterização e gênese do caráter coeso em latossolos amarelos e argissolos dos tabuleiros costeiros do Estado de Alagoas. **Revista Brasileira de Ciência do Solo**, Viçosa, MG, v. 33, n. 4, p. 1001–1011, 2009.

LUGASSI, R.; BEN-DOR, E.; ESHEL, G. Reflectance spectroscopy of soils post-heating-assessing thermal alterations in soil minerals. **Geoderma**, Amsterdam, v. 213, p. 268–279, 2014.

MA, F. *et al.* Investigation of soil properties using different techniques of mid-infrared spectroscopy. **European Journal of Soil Science**, Oxford, v. 70, n. 1, p. 96–106, 2019.

MADARI, Beáta E. *et al.* Mid- and near-infrared spectroscopic assessment of soil compositional parameters and structural indices in two Ferralsols. **Geoderma**, Amsterdam, v. 136, n. 1/2, p. 245–259, 2006.

MADEIRA, J. *et al.* Spectral (MIR) determination of kaolinite and gibbsite contents in lateritic soils. **Comptes Rendus de l'Académie des Sciences de Paris. Série 2a: Sciences de la Terre et des Planètes**, Paris, v. 321, n. 2, p. 119-128, 1995.

MARTENS, Harald; NÆS, Tormod. Multivariate calibration. *In*: KOWALSKI, B. R. (ed.). **Chemometrics**: mathematics and statistics in chemistry. Dordrecht: Springer, 1984. (ASIC, volume 138). p. 147–156.

MCCARTY, Gregory W.; REEVES, James B. Comparison of near infrared and mid infrared diffuse reflectance spectroscopy for field-scale measurement of soil fertility parameters. **Soil Science**, New Brunswick, v. 171, n. 2, p. 94–102, 2006.

MEDEIROS, Paula Suélen C. *et al.* Genesis and classification of soils from granitic hills in southern Brazil. **Journal of South American Earth Sciences**, Amsterdam, v. 98, [art.] 102494, 2020.

MELO, V. F.; WYPYCH, F. Caulinita e haloisita. *In*: MELO, V. F.; ALLEONI, L. R. F. (ed.). **Química e mineralogia do solo:** Parte I - conceitos básicos. Viçosa, MG: SBCS, 2019. p. 427–524.

MINASNY, Budiman *et al.* Regional transferability of mid-infrared diffuse reflectance spectroscopic prediction for soil chemical properties. **Geoderma**, Amsterdam, v. 153, n. 1/2, p. 155–162, 2009.

MINASNY, Budiman; MCBRATNEY, Alex B. Regression rules as a tool for predicting soil properties from infrared reflectance spectroscopy. **Chemometrics and Intelligent Laboratory Systems**, Amsterdam, v. 94, n. 1, p. 72–79, 2008.

MOHANTY, Biswajita; GUPTA, Abhinav; DAS, Bhabani S. Estimation of weathering indices using spectral reflectance over visible to mid-infrared region. **Geoderma**, Amsterdam, v. 266, p. 111–119, 2016.

MORELLOS, Antonios *et al.* Machine learning based prediction of soil total nitrogen, organic carbon and moisture content by using VIS-NIR spectroscopy. **Biosystems Engineering**, London, v. 152, p. 104–116, 2016.

MUNAWAR, Agus Arip *et al.* Calibration models database of near infrared spectroscopy to predict agricultural soil fertility properties. **Data in Brief**, [Amsterdam], v. 30, [art.] 105469, [p. 1–12], 2020.

NANNI, Marcos Rafael; DEMATTÊ, José Alexandre M. Spectral reflectance methodology in comparison to traditional soil analysis. **Soil Science Society of America Journal**, Madison, v. 70, n. 2, p. 393-407, 2006.

NAYAK, Preeti Sagar; SINGH, B. K. Instrumental characterization of clay by XRF , XRD and FTIR. **Bulletin of Materials Science**, Bangalore, v. 30, n. 3, p. 235–238, 2007.

NGUYEN, Tam; JANIK, Leslie; RAUPACH, Maxwell. Diffuse Reflectance Infrared Fourier Transform (DRIFT) spectroscopy in soil studies. **Australian Journal of Soil Research**, Melbourne, v. 29, n. 1, p. 49–67, 1991.

O'ROUKE, S. M. *et al.* An assessment of model averaging to improve predictive power of portable vis-NIR and XRF for the determination of agronomic soil properties. **Geoderma**, Amsterdam, v. 279, p. 31–44, 2016.

OLIVEIRA, Jessica Souza *et al*. Soil properties governing phosphorus adsorption in soils of Southern Brazil. **Geoderma Regional**, Amsterdam, v. 22, [art.] e00318, [p. 1–13], 2020.

OMRAN, E. S. E. Rapid prediction of soil mineralogy using imaging spectroscopy. **Eurasian Soil Science**, New York, v. 50, n. 5, p. 597–612, 2017.

PENG, Yi *et al*. Quantification of SOC and clay content using visible near-infrared reflectance-mid-infrared reflectance spectroscopy with jack-knifing partial least squares regression. **Soil Science**, New Brunswick, v. 179, n. 7, p. 325–332, 2014.

PINHEIRO, Érika F. M. *et al.* Prediction of soil physical and chemical properties by visible and near-infrared diffuse reflectance spectroscopy in the Central Amazon. **Remote Sensing**, Basel, v. 9, n. 4, p. 1–22, 2017.

POPPIEL, Raúl R. *et al.* Pedology and soil class mapping from proximal and remote sensed data. **Geoderma**, Amsterdam, v. 348, p. 189–206, 2019.

PRADO, Elias Martins Guerra *et al.* Reflectance spectroradiometry applied to a semi-quantitative analysis of the mineralogy of the N4ws deposit, Carajás Mineral Province, Pará, Brazil. **Ore Geology Reviews**, Amsterdam, v. 78, p. 101–119, 2016.

R DEVELOPMENT CORE TEAM. **R:** a language and environment for statistical computing. Vienna: R DEVELOPMENT CORE TEAM, 2005. Disponível em: https://www.r-project.org/. Acesso em: 10 set. 2018

RAMAROSON, Volaniaina H. *et al.* Mineralogical analysis of ferralitic soils in Madagascar using NIR spectroscopy. **Catena**, Cremlingen, v. 168, p. 106-108,

2018.

REATTO, A. *et al*. Caracterização mineralógica, potencial de reserva e sustentabilidade agrícola de alguns sítios florestais de eucalipto da região do Vale do Rio Doce (MG). **Revista Brasileira de Ciência do Solo**, Viçosa, MG, v. 22, n. 2, p. 255–266, 1998.

RODRÍGUEZ, J. M.; FERNÁNDEZ, J. A. Application of the second derivative of the Kubelka-Munk function to the semiquantitative analysis of Roman paintings. **Color Research and Application**, New York, v. 30, n. 6, p. 448–456, 2005.

SACRISTÁN, Daniel; VISCARRA ROSSEL, Raphael A.; RECATALÁ, Luis. Proximal sensing of Cu in soil and lettuce using portable X-ray fluorescence spectrometry. **Geoderma**, Amsterdam, v. 265, p. 6–11, 2016.

SAIKIA, Bhaskar J.; PARTHASARATHY, Gopalakrishnarao. Fourier transform infrared spectroscopic characterization of kaolinite from Assam and Meghalaya, Northeastern India. **Journal of Modern Physics**, Irvine, v. 1, p. 206–210, 2010.

SALISBURY, John W.; D'ARIA, Dana M. Emissivity of terrestrial materials in the 8-14 μm atmospheric window. **Remote Sensing of Environment**, New York, v. 42, p. 83–106, 1992.

SANTOS, Pablo Grahl; ALMEIDA, Jaime Antonio; SEQUINATTO, Letícia. Mineralogy of the clay fraction and chemical properties of soils developed from sedimentary lithologies of Pirambóia, Sanga-the-Cabral and Guará geological formations in southern Brazil. **Revista Brasileira de Ciência do Solo**, Viçosa, MG, v. 41, p. 1–19, 2017.

SAVITZKY, A.; GOLAY, M. J. E. Smoothing and differentiation of data by simplified least squares procedures. **Analytical Chemistry**, Washington, DC, v. 36, n. 8, p. 1627–1639, 1964.

SCHEINOST, A. C. *et al.* Use and limitations of second-derivative diffuse reflectance spectroscopy in the visible to near-infrared range to identify and quantify Fe oxide minerals in soils. **Clays and Clay Minerals**, Long Island City, v. 46, n. 5, p. 528–536, 1998.

SCHULZE, Darrell G. An introduction to soil mineralogy. *In*: DIXON, J. B.; SCHULZE, D. G. (ed.). **Soil mineralogy with environmental applications**. Madison: Soil Science Society of America, 2002. v. 7. (SSSA Book Series). cap. 1, p. 1-35.

SCHWERTMANN, U. Relations between iron oxides, soil color, and soil formation. *In*: BIGHAM, J. M.; CIOLKOSZ, E. J. (ed.). **Soil color**. Madison: Soil Science Society of America,1993. v. 31, cap. 4, p. 51–69.

SELLITTO, V. M. *et al.* Comparing two different spectroscopic techniques for the characterization of soil iron oxides: diffuse versus bi-directional reflectance. **Geoderma**, Amsterdam, v. 149, n. 1/2, p. 2–9, 2009.

SHI, Tiezhu *et al.* Improving the prediction of arsenic contents in agricultural soils by combining the reflectance spectroscopy of soils and rice plants. **International Journal of Applied Earth Observation and Geoinformation**, Washington, DC, v. 52, p. 95–103, 2016.

SILVA, Elisângela Benedet *et al*. A regional legacy soil dataset for prediction of sand and clay content with Vis-Nir-Swir, in Southern Brazil. **Revista Brasileira de Ciência do Solo**, Viçosa, MG, v. 43, [art.] e0180174, 2019.

SILVA, Luís Fernando *et al.* Soil variability in different landscape positions in the Porto Alegre botanical garden, southern Brazil. **Ciência e Agrotecnologia**, Lavras, v. 39, n. 5, p. 477–487, 2015.

SILVERO, Nélida Elizabet *et al.* Effects of water, organic matter, and iron forms in mid-IR spectra of soils: assessments from laboratory to satellite-simulated data. **Geoderma**, Amsterdam, v. 375, p. 1-14, 2020.

SIQUEIRA, D. S. *et al.* Detailed mapping unit design based on soil-landscape relation and spatial variability of magnetic susceptibility and soil color. **Catena**, Cremlingen, v. 135, p. 149–162, 2015.

SORIANO-DISLA, José M. *et al.* The performance of visible, near-, and mid-infrared reflectance spectroscopy for prediction of soil physical, chemical, and biological properties. **Applied Spectroscopy Reviews**, New York, v. 49, n. 2, p. 139–186, 2014.

STENBERG, Bo *et al.* Visible and near infrared spectroscopy in soil science. **Advances in Astronomy**, San Diego, v. 107, p. 163-215, 2010.

STENBERG, Bo. Effects of soil sample pretreatments and standardised rewetting as interacted with sand classes on Vis-NIR predictions of clay and soil organic carbon. **Geoderma**, Amsterdam, v. 158, n. 1/2, p. 15–22, 2010.

STEVENS, Antoine; RAMIREZ-LOPEZ, Leonardo. **An introduction to the prospectr package**. [*S.l.*: R Package], 2014.

SUN, Weichao; ZHANG, Xia. Estimating soil zinc concentrations using reflectance spectroscopy. **International Journal of Applied Earth Observation and Geoinformation**, Washington, DC, v. 58, p. 126–133, 2017.

TEIXEIRA, Paulo César *et al.* **Manual de métodos de análise de solo**. 3. ed. rev. e ampl. Brasília, DF: Embrapa, 2017.

TERRA, Fabrício S.; DEMATTÊ, José A. M.; VISCARRA ROSSEL, Raphael A. Spectral libraries for quantitative analyses of tropical Brazilian soils: comparing vis-NIR and mid-IR reflectance data. **Geoderma**, Amsterdam, v. 255/256, p. 81–93, 2015.

TERRA, Fabrício S.; DEMATTÊ, José A. M.; VISCARRA ROSSEL, Raphael A. Proximal spectral sensing in pedological assessments: vis–NIR spectra for soil classification based on weathering and pedogenesis. **Geoderma**, Amsterdam,

v. 318, p. 123–136, 2018.

TERRA, Silva. **Espectroscopia de reflectância do visível ao infravermelho médio aplicada aos estudos qualitativos e quantitativos de solo**. 2011. Tese (Doutorado) - Escola Superior de Agricultura Luiz de Queiroz, Universidade de São Paulo, Piracicaba, 2011.

TINTI, Anna *et al.* Recent applications of vibrational mid-Infrared (IR) spectroscopy for studying soil components: a review. **Journal of Central European Agriculture**, Zagreb, v. 16, n. 1, p. 1–22, 2015.

TORRENT, J.; BARRÓN, V. Diffuse reflectance spectroscopy of iron oxides. *In*: HUBBARD, Arthur T. (ed.). **Encyclopedia of Surface and Colloid Science**. New York: CRC, 2002. p. 1438–1446.

TOTSCHE, Kai Uwe *et al.* Microaggregates in soils. **Journal of Plant Nutrition and Soil Science**, Weinheim, v. 181, n. 1, p. 104–136, 2018.

TÜMSAVAŞ, Zeynal *et al.* Prediction and mapping of soil clay and sand contents using visible and near-infrared spectroscopy. **Biosystems Engineering**, London, v. 177, p. 90-100, 2019.

VAŠÁT, Radim *et al.* Combining reflectance spectroscopy and the digital elevation model for soil oxidizable carbon estimation. **Geoderma**, Amsterdam, v. 303, p. 133–142, 2017a.

VAŠÁT, Radim *et al.* Simple but efficient signal pre-processing in soil organic carbon spectroscopic estimation. **Geoderma**, Amsterdam, v. 298, p. 46–53, 2017b.

VASAVA, Hitesh B. *et al.* Assessment of soil texture from spectral reflectance data of bulk soil samples and their dry-sieved aggregate size fractions. **Geoderma**, Amsterdam, v. 337, p. 914–926, 2019.

VENDRAME, P. R. S. *et al.* The potential of NIR spectroscopy to predict soil texture and mineralogy in Cerrado Latosols. **European Journal of Soil Science**, Oxford, v. 63, n. 5, p. 743–753, 2012.

VENDRAME, P. R. S. *et al.* Formas de ferro e alumínio e suas relações com textura, mineralogia e carbono orgânico em Latossolos do cerrado. **Semina: Ciências Agrárias**, Londrina, v. 32, p. 1657–1666, 2011. Supl. 1.

VISCARRA ROSSEL, R. A. *et al.* Visible, near infrared, mid infrared or combined diffuse reflectance spectroscopy for simultaneous assessment of various soil properties. **Geoderma**, Amsterdam, v. 131, n. 1/2, p. 59–75, 2006.

VISCARRA ROSSEL, R. A. *et al.* In situ measurements of soil colour, mineral composition and clay content by vis-NIR spectroscopy. **Geoderma**, Amsterdam, v. 150, n. 3/4, p. 253–266, 2009.

VISCARRA ROSSEL, R. A. *et al.* Mapping iron oxides and the color of

Australian soil using visible-near-infrared reflectance spectra. **Journal of Geophysical Research: Earth Surface**, Hoboken, v. 115, n. F4, [art.] F04031, [p. 1–13], 2010.

VISCARRA ROSSEL, R. A. *et al.* Proximal soil sensing: an effective approach for soil measurements in space and time. **Advances in Agronomy**, San Diego, v. 113, p. 243-291, 2011.

VISCARRA ROSSEL, R. A. *et al.* A global spectral library to characterize the world's soil. **Earth-Science Reviews**, Amsterdam, v. 155, p. 198–230, 2016.

VISCARRA ROSSEL, R. A.; BEHRENS, T. Using data mining to model and interpret soil diffuse reflectance spectra. **Geoderma**, Amsterdam, v. 158, n. 1/2, p. 46–54, 2010.

WANG, Shan-qin *et al*. Prediction of soil texture using FT-NIR spectroscopy and pXRF spectrometry with data fusion. **Soil Science**, New Brunswick, v. 178, n. 11, p. 626–638, 2014.

WIGHT, Jason P.; ASHWORTH, Amanda J.; ALLEN, Fred L. Organic substrate, clay type, texture, and water influence on NIR carbon measurements. **Geoderma**, Amsterdam, v. 261, p. 36–43, 2016.

WIJEWARDANE, Nuwan K. *et al*. Predicting physical and chemical properties of us soils with a mid-infrared reflectance spectral library. **Soil Science Society of America Journal**, Madison, v. 82, n. 3, p. 722-731, 2018.

WREGE, Marcos Silveira *et al.* **Atlas climático da região sul do Brasil :** Estados do Paraná, Santa Catarina e Rio Grande do Sul. 2. ed. Pelotas: Embrapa Clima Temperado; Colombo: Embrapa Florestas, 2012. Disponível em: https://www.infoteca.cnptia.embrapa.br/infoteca/handle/doc/1045852. Acesso em: 2 maio 2019.

XU, Shengxiang *et al.* Determination of rice root density from Vis–NIR spectroscopy by support vector machine regression and spectral variable selection techniques. **Catena**, Cremlingen, v. 157, p. 12–23, 2017.

YU, Fang; HUNT, Allen Gerhard. Predicting soil formation on the basis of transport-limited chemical weathering. **Geomorphology**, Amsterdam, v. 301, p. 21–27, 2018.

ZHANG, Yakun *et al*. Depth-specific prediction of soil properties in situ using vis-NIR spectroscopy. **Soil Science Society of America Journal**, Madison, v. 81, n. 5, p. 993–1004, 2017.

ZHAO, Dongxue *et al*. A Vis-NIR spectral library to predict clay in Australian cotton growing soil. **Soil Science Society of America Journal**, Madison, v. 82, n. 6, p. 1347–1357, 2018.

ZHAO, Lulu *et al.* Assessing the utility of visible-to-shortwave infrared reflectance spectroscopy for analysis of soil weathering intensity and

paleoclimate reconstruction. **Palaeogeography, Palaeoclimatology, Palaeoecology**, Amsterdam, v. 512, p. 80–94, 2017.

ZHENG, Guanghui *et al.* Estimation of organic matter content in coastal soil using reflectance spectroscopy. **Pedosphere**, Beijing, v. 26, n. 1, p. 130–136, 2016.

ZHU, Yuanda; WEINDORF, David C.; ZHANG, Wentai. Characterizing soils using a portable X-ray fluorescence spectrometer: 1. Soil texture. **Geoderma**, Amsterdam, v. 167/168, p. 167–177, 2011.

7. APÊNDICES

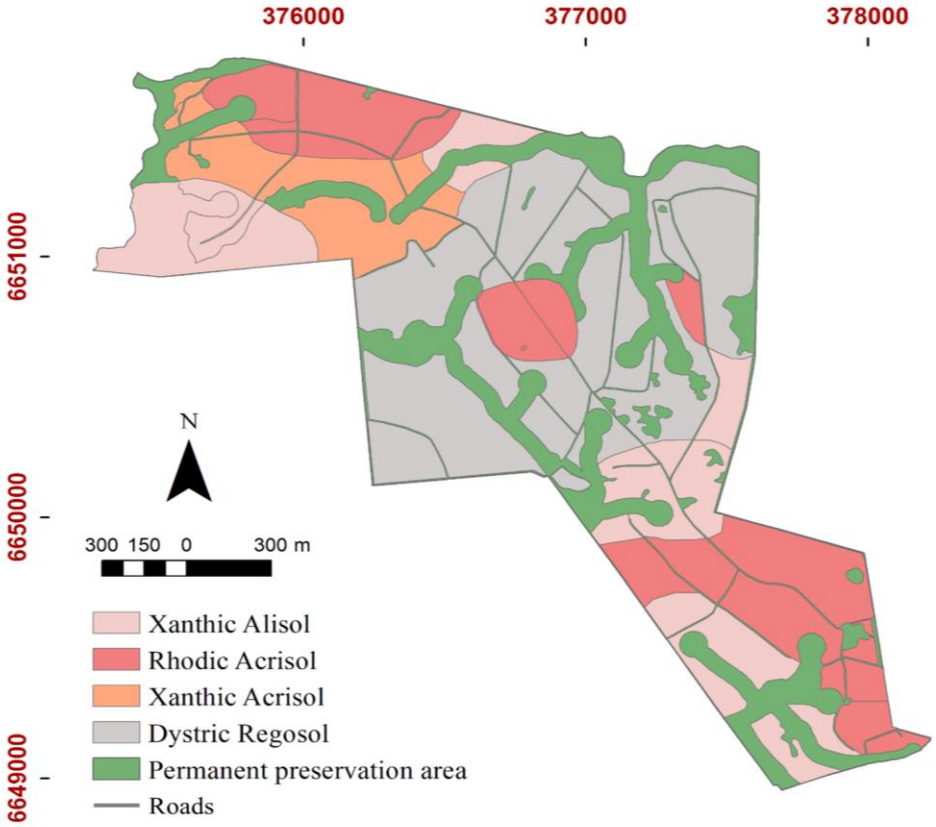

Apêndice 1. Mapa de solos da área de estudo e localização das áreas de preservação permanente

Apêndice 2. Proporção dos minerais das 197 amostras de solo

Pontos amostrais	Profundidade (cm)	Gt	Hm	Kt (%)	Il	Ch
1	0-20	31.2	38.7	24.5	1.7	3.9
	20-40	40.5	28.6	25.3	1.4	4.2
	40-60	45.6	29.3	19.9	1.5	3.7
2	0-20	44.1	29.7	18.4	3.6	4.2
	20-40	48.5	28.1	19.1	1.2	3.1
3	0-20	42.3	22.5	25.2	3.5	6.5
	20-40	46.4	24.4	24.2	1.5	3.5
	40-60	28.8	20.8	39.4	4	7
4	0-20	45.1	14.5	29.4	4.3	6.7
	20-40	45.8	14.7	31.9	2.6	5
	40-60	42.2	16.1	32.9	2.7	6.1
5	0-20	51.6	14.7	25.7	3.8	4.2
	20-40	59	9.9	25.8	1.9	3.4
	40-60	48.2	13.2	30.5	2.5	5.6
6	0-20	50.7	28.4	13.7	2.8	4.4
	20-40	50.2	29.1	16.3	1.9	2.5
	40-60	51.9	26.9	16.6	1.7	2.9
7	0-20	59.3	15.5	21.4	1.9	1.9
	20-40	51	13.4	25.4	4	6.2
	40-60	56.3	13.9	25.5	1.5	2.8
8	0-20	46.9	33.6	14.6	1.9	3
	20-40	43.5	32.7	17.9	1.9	4
	40-60	42.3	30	21.8	1.8	4.1
9	0-20	72.9	4.2	17.5	1.9	3.5
	20-40	69.6	2.7	20.4	2.7	4.6
	40-60	65.8	3.5	23.6	2.3	4.8
10	0-20	48.9	6.1	34.5	4.5	6
	20-40	60	0.4	30.4	2.7	6.5
	40-60	60	5.8	25.9	2.6	5.7
11	0-20	40.1	5.8	34.2	8.9	11
	20-40	55.3	1.8	31.7	4.4	6.8
	40-60	47.7	7.7	34.1	2.9	7.6
12	0-20	42	5.3	31.8	10.5	10.4
	20-40	53.4	1.2	30.8	6.5	8.1
	40-60	52.1	0.4	32.4	6.5	8.6
13	0-20	47	24.8	18.6	3.8	5.8
	20-40	45.1	27.1	19.6	3.5	4.7
	40-60	47.9	26.4	19.4	2	4.3
14	0-20	49.4	32.2	13.5	1.7	3.2
	20-40	39	37.4	17.6	2.5	3.5
	40-60	48.7	28.7	17.4	1.7	3.5
15	0-20	47.9	29.8	17.5	1.2	3.6
	20-40	42.2	30.9	22	1.8	3.1
	40-60	46.9	26.7	21.6	1.7	3.1
16	0-20	51	13.5	23.4	4.9	7.2
	20-40	53	17.6	24.1	1.6	3.7
	40-60	56	19.5	20.3	1.4	2.8
17	0-20	47.4	33.8	14.1	1.5	3.2
	20-40	46.5	31.3	14.3	3.4	4.5
	40-60	49.4	31.7	14.9	1.2	2.8
18	0-20	43.7	36.4	16.6	1.2	2.1
	20-40	49.3	34	14.1	0.5	2.1
	40-60	47.2	32.2	15.7	1.7	3.2
19	0-20	34.8	8.9	39.6	5.7	11
	20-40	40.8	3.5	41.2	5.3	9.2
	40-60	48	0	38.8	5.8	7.4
20	0-20	57.5	2.7	30.5	3.7	5.6
	20-40	63.7	2.6	25	3.3	5.4
	40-60	57.1	10.6	26.7	1.9	3.7
21	0-20	54.7	18.6	22	1.7	3
	20-40	41.1	18.5	30.7	3.8	5.9
	40-60	32.1	19.8	37.1	4	7
22	0-20	55.6	10.9	26.2	2.5	4.8
	20-40	61.8	5.8	26.8	2.2	3.4
	40-60	70	1.4	22.7	2.2	3.7
23	0-20	45.8	32.9	17.9	1.3	2.1
	20-40	39.2	35.4	18.6	3.4	3.4
	40-60	42	34.5	18.6	1.6	3.3
24	0-20	45	24.4	26	1.8	2.8
	20-40	38.3	23.1	29.9	3.4	5.3

	40-60	38.8	23.5	28.1	3.5	6.1
25	0-20	51.2	20.7	21.4	2.4	4.3
	20-40	56.4	20.8	18.6	1.5	2.7
	40-60	34.5	23.4	30.7	3.9	7.5
26	0-20	37.4	8.9	44.1	3.5	6.1
	20-40	37.7	5.8	45.9	3.7	6.9
	40-60	50.8	6.6	34.4	3.5	4.7
27	0-20	51.7	10.4	30.8	2.3	4.8
	20-40	41.2	11.4	36.6	4	6.8
	40-60	39.9	16.2	34.8	3	6.1
28	0-20	58.1	17.5	20.7	1.5	2.2
	20-40	48	20.9	25.8	1.8	3.5
	40-60	40	23.6	30.7	1.9	3.8
29	0-20	54.5	25.2	18.6	0.4	1.3
	20-40	47.4	27.4	19.9	1.9	3.4
	40-60	49.7	25.1	19.2	2.4	3.6
30	0-20	37.3	28.2	23.1	4.6	6.8
	20-40	37.6	27.6	25.2	3.6	6
	40-60	35.7	30.5	25.9	2.6	5.3
31	0-20	71.5	8.1	15.8	1.6	3
	20-40	75.3	6.9	12.2	2.1	3.5
	40-60	76.8	7.9	12	0.8	2.5
32	0-20	53.2	17.9	22.5	2.7	3.7
	20-40	54.9	9.5	28.6	2.5	4.5
	40-60	42.8	4.3	41.3	4.1	7.5
33	0-20	51.3	19.3	24.7	1.4	3.3
	20-40	53.2	20.1	24.5	0.3	1.9
	40-60	41.1	21	28.1	3.3	6.5
34	0-20	53.6	22.3	18.2	2.2	3.7
	20-40	57.9	17.7	16.1	3.1	5.2
	40-60	53.6	21.4	18.4	2.1	4.5
35	0-20	45.4	21.8	24.6	2.8	5.4
	20-40	29.2	23.2	38.4	2.9	6.3
	40-60	37.5	26.5	28.2	2.5	5.3
36	0-20	63.8	14.1	19.4	0.9	1.8
	20-40	40.1	19.4	31.5	2.9	6.1
	40-60	37.1	16.5	36.6	3.4	6.4
37	0-20	48	5.5	32.7	5.8	8
	20-40	57.2	4.1	27.1	4.8	6.8
	40-60	46.6	3.8	35.4	4.2	10
38	0-20	51.3	20.3	20.5	2.9	5
	20-40	45.3	22	22.7	3.9	6.1
	40-60	41.1	25	26.1	3.1	4.7
39	0-20	55.4	8.3	29.9	2.4	4
	20-40	45.6	4.5	35.5	5.4	9
	40-60	57.8	2.5	28.6	4.6	6.5
40	0-20	48.6	15.6	24.3	4.1	7.4
	20-40	49.5	17.1	26.8	2.1	4.5
	40-60	37	18.2	35.6	3.4	5.8
41	0-20	47.6	23.2	24.1	1.8	3.3
	20-40	42.3	25	25.3	2.1	5.3
	40-60	34.2	26.4	32	2.3	5.1
42	0-20	57.2	9.9	28.1	1.5	3.3
	20-40	42.8	17.2	31	3	6
	40-60	35.8	26.1	31.6	1.8	4.7
43	0-20	49.7	13.5	28.6	3	5.2
	20-40	45.4	17.1	30.4	2.4	4.7
	40-60	49.5	16.6	27.7	2.1	4.1
44	0-20	47.3	5.7	31	7.1	8.9
	20-40	54.3	3.6	34.5	3.1	4.5
	40-60	63	3.9	24.6	2.9	5.6
45	0-20	62.4	8.6	24.2	1.1	3.7
	20-40	55.4	6.5	27.2	4.1	6.8
	40-60	59.2	8.1	25.9	2.6	4.2
46	0-20	54.4	21.7	17.3	3.1	3.5
	20-40	51.8	24.3	18.6	1.9	3.4
	40-60	54	21.5	20.2	1.5	2.8
47	0-20	66.7	6.3	20.2	2.5	4.3
	20-40	62.6	6.1	26.6	1.8	2.9
	40-60	59.6	7.3	24.9	2.8	5.4
48	0-20	1.6	1.6	70.3	11.6	14.9
	20-40	36.4	8.2	42.3	3.9	9.2
	40-60	51.9	1.8	37.4	3.1	5.8
49	0-20	66.7	2	26.3	1.5	3.5
	20-40	52	10.5	31.1	2.3	4.1

	40-60	52.8	17.5	23.9	2.2	3.6
50	0-20	40.6	27.1	22.9	3.7	5.7
	20-40	34.8	29.3	27.6	2.9	5.4
	40-60	23.2	35.7	31.5	3.4	6.2
51	0-20	53.4	18.5	20	3.1	5
	20-40	51.1	19	19.7	4.3	5.9
	40-60	59	20.3	17.4	1.4	1.9
52	0-20	41.6	25.4	24.9	3.1	5
	20-40	40.9	29.2	23.3	2.7	3.9
	40-60	29.1	29.2	29.9	4.7	7.1
53	0-20	46	33.9	16.9	1.2	2
	20-40	39.2	34.3	20.9	2	3.6
	40-60	44.8	25.7	22.1	2.6	4.8
54	0-20	48	33.7	13.3	1.8	3.2
	20-40	45.5	36.7	13.9	1	2.9
	40-60	48.2	32.3	15.6	1.5	2.4
55	0-20	37	28.1	26.3	3.3	5.3
	20-40	25.2	29.4	36.5	3.2	5.7
	40-60	37.5	26	27.9	2.8	5.8
56	0-20	46.5	29.2	19.4	1.5	3.4
	20-40	36.7	32.5	24.1	2.3	4.4
	40-60	35.9	27.9	26	3.9	6.3
57	0-20	60.3	6	28.9	2.1	2.7
	20-40	60.1	8.4	26.1	2.1	3.3
	40-60	59.2	6.8	28.3	2.1	3.6
58	0-20	48.2	24.4	18.5	4	4.9
	20-40	44.5	27.6	20.4	3.3	4.2
	40-60	52.6	21.7	19.2	2.5	4
59	0-20	41.8	15	35.2	2.9	5.1
	20-40	44.2	12.3	32.7	4.3	6.5
	40-60	28.4	8.6	51.1	5.1	6.8
60	0-20	51.5	19.7	22.5	2.6	3.7
	20-40	48	22.9	22.6	2.8	3.7
	40-60	49.1	27.3	19.9	1.1	2.6
61	0-20	46.2	28.9	18.8	2.3	3.8
	20-40	40.3	30.5	21.4	2.8	5
	40-60	37.8	28.9	25.9	2.3	5.1
62	0-20	53.4	21.1	18.5	2.7	4.3
	20-40	41.2	25.7	27	2	4.1
	40-60	41.1	21.7	30.5	2.4	4.3
63	0-20	58.9	5.7	26.6	2.8	6
	20-40	56	7.6	28.6	2.7	5.1
	40-60	45.3	12.5	33.5	2.5	6.2
64	0-20	53.7	12.4	24.3	4	5.6
	20-40	52.6	14.1	25.6	3.1	4.6
	40-60	37.2	14	35.8	5.2	7.8
65	0-20	48	25.9	19.4	3	3.7
	20-40	53.5	22.4	18.2	2.2	3.7
	40-60	41.3	30.4	19.8	3.3	5.2
66	0-20	49.8	17.6	25.6	2.9	4.1
	20-40	43.9	19.6	28.6	2.4	5.5
	40-60	32.9	24.3	32.4	4.1	6.3